



# HHS Public Access

Author manuscript

Cell Rep. Author manuscript; available in PMC 2022 June 17.

Published in final edited form as:

Cell Rep. 2022 May 24; 39(8): 110856. doi:10.1016/j.celrep.2022.110856.

## DDX41 is required for cGAS-STING activation against DNA virus infection

Ravi Shankar Singh<sup>1</sup>,  
Venkatasubramanian Vidhyasagar<sup>1</sup>,  
Shizhuo Yang<sup>1</sup>,  
Ananna Bhadra Arna<sup>1</sup>,  
Manisha Yadav<sup>1</sup>,  
Aanchal Aggarwal<sup>1</sup>,  
Alexya N. Aguilera<sup>2</sup>,  
Satoru Shinriki<sup>3</sup>,  
Kalpana Kalyanasundaram Bhanumathy<sup>4</sup>,  
Kannupriya Pandey<sup>5</sup>,  
Aizhang Xu<sup>4</sup>,  
Noreen Rapin<sup>6</sup>,  
Mark Bosch<sup>4</sup>,  
John DeCoteau<sup>7</sup>,  
Jim Xiang<sup>4</sup>,  
Franco J. Vizeacoumar<sup>4,7</sup>,  
Yan Zhou<sup>5,6</sup>,  
Vikram Misra<sup>6</sup>,  
Hirotaka Matsui<sup>3</sup>,  
Susan R. Ross<sup>2</sup>,  
Yuliang Wu<sup>1,8,\*</sup>

<sup>1</sup>Department of Biochemistry, Microbiology and Immunology, University of Saskatchewan, Saskatoon SK S7N 5E5, Canada

This is an open access article under the CC BY-NC-ND license (<http://creativecommons.org/licenses/by-nc-nd/4.0/>).

\*Correspondence: [yuliang.wu@usask.ca](mailto:yuliang.wu@usask.ca).

### AUTHOR CONTRIBUTIONS

R.S.S. performed the majority of the experiments; V.V., S.Y., A.B.A., M.Y., and A.A. performed some experiments and provided intellectual input. K.K.B. and F.J.V. contributed to the lentivirus work. N.R. and V.M. contributed to the HSV-1 virus work. K.P. and Y.Z. contributed to the IAV virus work. A.N.A. and S.R.R. contributed to the Ddx41-KO mouse work. S.S. and H.M. collected patient samples and performed RNA-seq. A.X. and J.X. contributed to bone marrow differentiation. M.B. and J.D. consulted on MDS/AML diseases. R.S.S. and Y.W. conceived of and coordinated the study and wrote the paper. All authors reviewed the results and approved the final version of the manuscript.

### SUPPLEMENTAL INFORMATION

Supplemental information can be found online at <https://doi.org/10.1016/j.celrep.2022.110856>.

### DECLARATION OF INTERESTS

The authors declare no conflicts of interest.

<sup>2</sup>Department of Microbiology and Immunology, College of Medicine, University of Illinois at Chicago, Chicago, IL, USA

<sup>3</sup>Department of Molecular Laboratory Medicine, Faculty of Life Sciences, Kumamoto University, Kumamoto, Japan

<sup>4</sup>Saskatchewan Cancer Agency, Saskatoon, SK S7N 5E5, Canada

<sup>5</sup>Vaccine and Infectious Disease Organization-International Vaccine Centre (VIDO-InterVac), University of Saskatchewan, Saskatoon, SK S7N 5E3, Canada

<sup>6</sup>Department of Veterinary Microbiology, Western College of Veterinary Medicine, University of Saskatchewan, Saskatoon, SK S7N 5B4, Canada

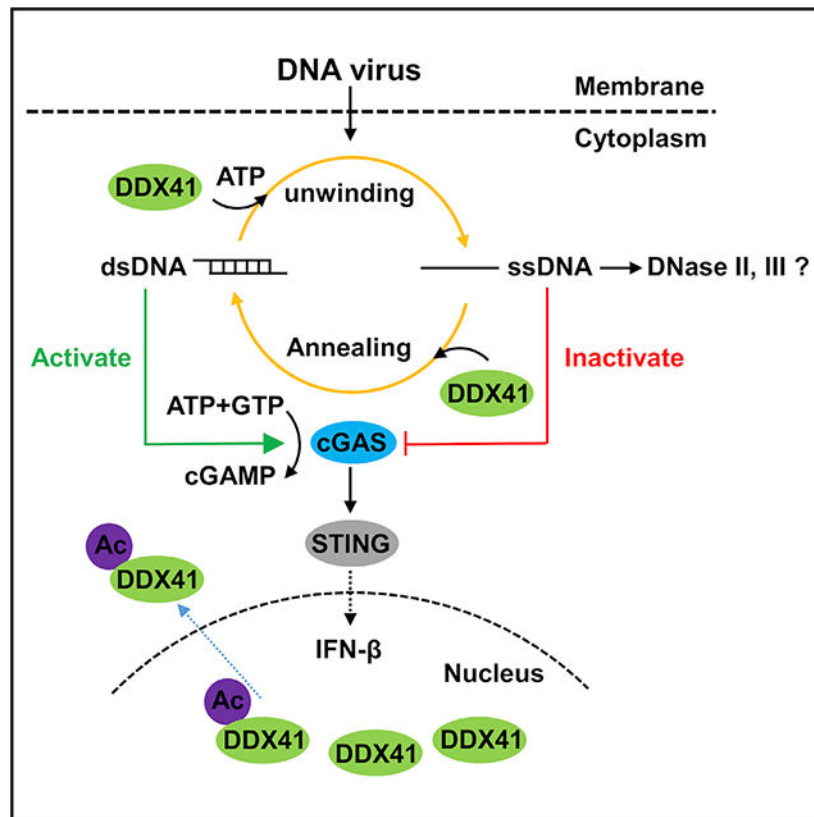
<sup>7</sup>Department of Pathology and Laboratory Medicine, University of Saskatchewan, Saskatoon, SK S7N 5E5, Canada

<sup>8</sup>Lead contact

## SUMMARY

Upon binding double-stranded DNA (dsDNA), cyclic GMP-AMP synthase (cGAS) is activated and initiates the cGAS-stimulator of IFN genes (STING)-type I interferon pathway. DEAD-box helicase 41 (DDX41) is a DEAD-box helicase, and mutations in DDX41 cause myelodysplastic syndromes (MDSs) and acute myeloid leukemia (AML). Here, we show that DDX41-knockout (KO) cells have reduced type I interferon production after DNA virus infection. Unexpectedly, activations of cGAS and STING are affected in DDX41 KO cells, suggesting that DDX41 functions upstream of cGAS. The recombinant DDX41 protein exhibits ATP-dependent DNA-unwinding activity and ATP-independent strand-annealing activity. The MDS/AML-derived mutant R525H has reduced unwinding activity but retains normal strand-annealing activity and stimulates greater cGAS dinucleotide-synthesis activity than wild-type DDX41. Overexpression of R525H in either DDX41-deficient or -proficient cells results in higher type I interferon production. Our results have led to the hypothesis that DDX41 utilizes its unwinding and annealing activities to regulate the homeostasis of dsDNA and single-stranded DNA (ssDNA), which, in turn, regulates cGAS-STING activation.

## Graphical Abstract



### In brief

cGAS is activated by dsDNA. Singh et al. find DDX41 regulates cGAS activation through unwinding and annealing activities on dsDNA and ssDNA, respectively, and MDS/AML patient mutant R525H causes overactivation of innate immune response due to its unbalanced activities. This DDX41-cGAS-STING pathway may be related to molecular pathogenesis of MDS/AML.

## INTRODUCTION

Innate immunity is a mechanism of host cells that provides the first line of defense against pathogenic invaders, such as viruses and bacteria. Immune cells utilize a germline-encoded innate immune sensor, termed pattern-recognition receptors (PRRs), to rapidly detect pathogenic invaders (Akira et al., 2006; Thompson et al., 2011). After ligand recognition, PRRs trigger intracellular cascades to elicit early innate immune responses, namely triggering signaling cascades that regulate gene expression and stimulate the production of type I interferons (IFNs), chemokines, and proinflammatory cytokines, which activate a broad anti-pathogenic immune response (Takeuchi and Akira, 2010). Cyclic GMP-AMP synthase (cGAS) is a PRR that recognizes cytosolic DNA (Ablasser and Chen, 2019). Binding with double-stranded DNA (dsDNA) (Kranzusch et al., 2013; Zhou et al., 2018; Xie et al., 2019), cGAS is activated and synthesizes the cyclic dinucleotide 2'3'-cGAMP that acts as a secondary messenger binding to the signaling adaptor stimulator of IFN genes (STING). Activated STING leads to the activation of TANK-binding kinase 1 (TBK1)

that phosphorylates and activates the transcription factor IFN regulatory factor 3 (IRF3), thus inducing IFN expression (Chen et al., 2016). Therefore, the innate immune response is an essential defense strategy for host cells; however, the timing and duration of these responses must be tightly regulated, as excessive production of type I IFNs will lead to proinflammatory or autoimmune diseases (Theofilopoulos et al., 2017). Very recently, cGAS was found to be auto-inhibited by nucleosomes through blocking dsDNA binding in the nucleus (Pathare et al., 2020; Zhao et al., 2020; Michalski et al., 2020; Boyer et al., 2020; Kujirai et al., 2020; Cao et al., 2020); however, it remains unknown how cGAS is regulated in the cytoplasm.

DEAD-box helicase 41 (DDX41) is a member of helicase superfamily 2. A DEAD-box helicase small interfering RNA (siRNA) screening found that DDX41 acted as an intracellular DNA sensor in myeloid dendritic cells (Zhang et al., 2011). Accumulating evidence suggests DDX41 plays a critical role in the STING-TBK1-IRF3-type I IFN signaling pathway (Parvatiyar et al., 2012; Soponpong et al., 2018; Ma et al., 2018; Stavrou et al., 2018; Zhang et al., 2013; Hu et al., 2020); however, other groups found that knockdown of DDX41 has little effect on IFN- $\beta$  induction in response to DNA stimulation or DNA virus infection (Abe et al., 2013; Sun et al., 2013). In addition to its role in innate immunity, both germline and acquired somatic mutations of DDX41 have been associated with myelodysplastic syndromes (MDSs) and/or acute myeloid leukemia (AML) (Cardoso et al., 2016; Ding et al., 2012; Abou Dalle et al., 2019; Hosono, 2019; Kim et al., 2020; Qu et al., 2020; Bannon et al., 2020; Choi et al., 2021; Fazio et al., 2021; Singhal et al., 2021; Goyal et al., 2021; Polprasert et al., 2020; Li et al., 2021; Yang et al., 2021; Alkhateeb et al., 2021; Churpek and Smith-Simmer, 1993; Duployez et al., 2022), chronic myeloid leukemia (CML) (Goyal et al., 2021), acute erythroid leukemia (AEL) (Iacobucci et al., 2019), and other hematolymphoid malignancies (Goyal et al., 2021; Singhal et al., 2021; Choi et al., 2021). The most frequently identified somatic mutation is c.1574G>A, p.R525H (Yoneyama-Hirozane et al., 2017; Lewinsohn et al., 2016; Polprasert et al., 2015; Singhal et al., 2021), which is confined to a highly conserved region of DDX41 and is thought to contribute to nucleotide coordination (Li et al., 2016). DDX41 mutations also lead to tumor-suppressor function due to altered pre-mRNA splicing, RNA processing, and inhibition of cell-cycle progression (Kadono et al., 2016; Lewinsohn et al., 2016; Polprasert et al., 2015; Tsukamoto et al., 2020). Thus, further studies are required to clarify the role of DDX41 in the DNA sensing pathway and its molecular pathogenesis leading to diseases.

## RESULTS

### DDX41 knockout cells have reduced cytokine responses to DNA virus infection

Knockdown of DDX41 in mouse and human cells inhibits the innate immune response and results in defective activation of STING (Zhang et al., 2011; Parvatiyar et al., 2012; Ma et al., 2015). To understand its role completely, we designed four guide RNAs for the CRISPR-Cas9 system to knock out (KO) the *DDX41* gene in human cell lines (Figure S1A). We started with HeLa cells and obtained two cell lines that lack detectable DDX41 protein (Figures 1A and S1B-S1E). Notably, the expression of cGAS, STING, TBK1, and IRF3

remained similar in the DDX41 KO compared with the wild-type (WT) cell line (Figure 1A).

To determine whether DDX41 KO cells are hindered in their ability to produce IFN- $\beta$  in response to exogenous DNA, we challenged the cells with poly(dA:dT) and examined IFN production, as well as individual steps in the cGAS-STING-IRF3-type I IFN signaling cascade, over a period of 24 h. qPCR showed that WT cells generated a robust IFN- $\beta$  (Figure 1B) and IFN-stimulated gene 56 (*ISG56*; Figure 1C) response that peaked at 6 h post treatment, while their expression was severely blunted in the two *DDX41*<sup>-/-</sup> clones. Next, we checked individual proteins and found that the expression of cGAS, as well as the phosphorylated STING, TBK1, and IRF3, started to increase after poly(dA:dT) stimulation and peaked in WT cells at 4 h for cGAS, 6 h for p-STING, 6–8 h for p-TBK1, and 8–12 h for p-IRF3 (Figures 1D and 1F–1I). In *DDX41*<sup>-/-</sup> cells, the expression of cGAS increased at 1 h and remained at higher expression up to 12 h then declined at 18–24 h; however, the phosphorylation of STING, TBK1, and IRF3 consistently declined (Figures 1E–1I).

Despite that HeLa cells have been used in many similar studies (Volkman et al., 2019; Sun et al., 2021; Wang et al., 2017), they are reportedly defective in DNA-induced IFN responses (Lau et al., 2015). We next conducted the above experiments in a THP-1 monocytic cell line that has a luciferase reporter gene under the control of an ISG54 minimal promoter in conjunction with five IFN-stimulated response elements (InvivoGen). Using the sgRNA-1 (Figure S1A) and a lentivirus delivery system, we generated a DDX41 KO THP-1 cell line (Figure 1J). After differentiating to macrophages with PMA, we transfected the macrophages with poly(dA:dT) and performed luciferase assays, qPCR for IFN- $\beta$  mRNA levels, and ELISA for IFN- $\beta$  proteins over a period of 0–24 h. Our results showed that poly(dA:dT) induced IFN- $\beta$  expression at both the mRNA (Figure 1K) and protein (Figure 1L) levels in WT cells, peaking at 6 to 8 and 12 h post transfection, respectively. However, DDX41-deficient cells exhibited a severely reduced response. A similar difference between these two cell lines was observed for *ISG56* gene expression (Figure 1M) and IFN-induced luciferase activity (Figure 1N). Furthermore, we evaluated the expression and activation of cGAS, STING, TBK1, and IRF3. Similar to the patterns found in HeLa cells, cGAS expression peaked at 2–4 h, and the presence of phosphorylated STING, TBK1, and IRF3 became apparent at 2 to 4 h and peaked at 4 to 6, 6 to 8, and 6 h, respectively, in *DDX41*<sup>+/+</sup> cells (Figures 1O and 1Q–1T). In contrast, the expression of cGAS increased at 1 and 2 h and diminished substantially at 8–24 h in *DDX41*<sup>-/-</sup> cells; however, the phosphorylation of STING, TBK1, and IRF3 was significantly reduced (Figures 1P–1T).

Because poly(dA:dT) could activate RNA sensor RIG-I and trigger the STING-IRF3-type I IFN signaling pathway (Ablasser et al., 2009), we then treated cells with short DNA (a vaccinia virus DNA motif [VACV 70-mer]) (Unterholzner et al., 2010) and long DNA (salmon-sperm DNA) and found increased cytokine responses post transfection in HeLa and THP-1 WT cells; however, DDX41-deficient cells exhibited a blunted response (Figures S2A–S2E). To further confirm that DDX41 acts as a DNA sensor, we infected THP-1 cells with a DNA virus (herpes simplex virus type 1 [HSV-1]) and found that DDX41-deficient cells had significantly reduced IFN- $\beta$  induction compared with WT cells (Figures S2F and S2G). Similar results were obtained for *ISG56* gene expression and luciferase activity

(Figures S2H and S2I). Next, we treated cells with dsRNA mimic poly(I:C) and found that, although *IFN-β* mRNA and protein levels increased in a dose-dependent manner (higher in 100 ng than in 10 ng), DDX41-deficient and WT cells showed no significant difference in terms of IFN-β expression (Figures S2J and S2K). Similarly, the expression of *ISG56* and luciferase in DDX41-deficient cells and WT cells did not differ (Figures S2L and S2M). We also infected the THP-1 cell lines with influenza A virus (IAV; MOI = 0.1, 1, and 10) and found that the RNA sensor RIG-I was upregulated upon IAV infection, so was the phosphorylated TBK1 (Figure S2N) and co-localization of RIG-I and MAVS (Figure S2O). However, IFN-β expression increased in both DDX41-deficient and -proficient cells, with no difference regardless of IAV dosage (Figures S2P and S2Q). We also discovered similar expression patterns of *ISG56* and luciferase in both cell lines infected by the RNA virus (Figures S2R and S2S), suggesting that DDX41 is a sensor for DNA but not RNA.

### DDX41 is required for the activation of cGAS and STING

To explore the reasons that cause reduced type I IFN production in DDX41 KO cells, we tested whether DDX41 deficiency affects the activation of cGAS and STING, the two key molecules in the innate immunity pathway. Using cGAS<sup>-/-</sup> as a negative control, we transfected WT and DDX41<sup>-/-</sup> THP-1 macrophages with poly(dA:dT) and salmon-sperm DNA, followed by measuring cGAMP in cell lysates using an ELISA kit (Cayman). Interestingly, DDX41<sup>-/-</sup> cells had significantly reduced cGAMP compared with WT cells in both DNA treatments, whereas cGAMP was completely abolished in cGAS<sup>-/-</sup> cells (Figure 2A). cGAS oligomerization is important for its activation after binding to dsDNA (Zhang et al., 2014); indeed, we found DDX41 deficiency significantly inhibited the self association of cGAS in THP-1 cells (Figure 2B) and HeLa cells (Figure S3A) after poly(dA:dT) stimulation.

Because DDX41 KO results in reduced STING activation, as indicated by S366 phosphorylation (Figures 1E, 1G, 1P, and 1R), we next asked whether DDX41 KO would affect STING's dimerization and subcellular localization, which are also essential for its function in innate immunity (Ouyang et al., 2012). To this end, we first examined the dimerization status of STING and found it migrated as an ~37 kDa monomer and an ~75 kDa dimer under non-reducing conditions (Figure 2C). Notably, DDX41 KO cells had reduced STING dimerization, particularly at 4–6 h post transfection, in both THP-1 and HeLa cells (Figures 2C and S3B). Next, we investigated the subcellular localization of STING and found it localized in the ER-Golgi intermediate compartment (ERGIC) after poly(dA:dT) stimulation (Figure 2D) and trafficked to the Golgi and perinuclear microsome (marked by the phosphorylated TBK1) in WT cells (Figures 2E and 2F); however, DDX41 deficiency markedly inhibited the transportation of STING to the ERGIC, Golgi, and perinuclear microsome. Collectively, our results suggest that DDX41 is required for the activation of cGAS and STING.

To extend our findings to primary cells of Ddx41 KO mice (Stavrou et al., 2018; Ma et al., 2022), we isolated bone marrow and differentiated it into macrophages (bone-marrow-derived macrophages [BMDMs]) and dendritic cells (bone-marrow-derived dendritic cells [BMDCs]) (Figure S4A), and Western blot confirmed the cell-type-specific loss of DDX41

(Figure S4B). Similar to the response to murine leukemia virus (MLV) and human immunodeficiency virus (HIV) (Stavrou et al., 2018), both BMDMs and BMDCs had reduced INF- $\beta$  expression in response to HSV-1 infection (Figure S4C). Moreover, we found that the key molecules (phosphorylated STING, TBK1, and IRF3) were reduced or completely abolished in Ddx41 KO cells (Figure 2G). In addition, cGAMP (Figure 2H), cGAS oligomerization (Figure 2I), and STING dimerization (Figure 2J) were reduced in Ddx41 KO BMDMs and BMDCs after HSV-1 infection. Ddx41 deficiency also markedly inhibited the trafficking of Sting to the ERGIC (Figure 2K) and Golgi (Figure 2L) in BMDMs infected by HSV-1, further confirming that DDX41 is required for the activation of cGAS and STING.

### **DDX41 protein has ATP-dependent DNA-unwinding activity and ATP-independent strand-annealing activity**

According to its primary protein sequence, DDX41 is a DEAD-box RNA helicase (Lewinsohn et al., 2016; Omura et al., 2016); however, the literature and our results suggest that DDX41 is not involved in IFN production in response to RNA transfection or RNA virus infection (Zhang et al., 2011). To investigate its biochemical properties, we expressed recombinant DDX41 protein in bacteria (DE3), purified it by chromatographic methods, and verified it by western blotting (Figure 3A and S5A-S5E). DDX41 exists as a monomer with a mass of 67.97 kDa. Using a 3'- and 5'-tailed 13-bp duplex RNA commonly used with DEAD-box proteins (Tanu et al., 2017), we found DDX41 could not unwind these substrates (Figures 3B and 3C). In contrast, another DEAD-box helicase, DDX43, displayed a strong unwinding activity (last lane), as we previously reported (Tanu et al., 2017; Yadav et al., 2020).

Our results suggest that DDX41 is required for IFN production in response to DNA or DNA viruses (Figures 1 and S2). Many helicases possess dual unwinding activity, acting on both DNA and RNA substrates (Pyle, 2008). Thus, we asked whether DDX41 can unwind DNA substrates. We found that DDX41 can efficiently unwind a 20-bp forked duplex DNA substrate (Figure 3D). Interestingly, it preferred to act on a 3'- versus 5'-tailed duplex DNA substrate (Figures 3E and 3F) and was inactive on a blunt-end duplex DNA substrate (Figure 3G). Efficient unwinding activity was observed with ATP and dATP (to a lesser extent; Figure 3H) but not with non-hydrolyzable ATP analogs ATP  $\gamma$  S or AMP-PNP (Figure 3I). Collectively, our data indicate that DDX41 unwinds duplex DNA in the 3' to 5' direction and in an ATP-dependent manner. Electrophoretic mobility shift assay (EMSA) revealed that DDX41 exhibited binding affinity in the order DNA > DNA:RNA hybrid > RNA (Figures S5F-S5H). We also examined its unwinding activity on longer duplex DNA substrates to further assess its processivity and found that DDX41 could unwind 30-, 40-, and 50-bp forked duplex substrates but noted less unwinding with increasing duplex length (Figures S5I-S5L). During the unwinding assays, we constantly observed that the DDX41 protein could rewind the DNA substrates at a high concentration (Figures 3D and S5I-S5L). To confirm that the unwinding activity detected was truly dependent on DDX41 and was not due to contaminants in the preparation of the DDX41 protein, we changed the conserved glutamic acid 345 to alanine (E345A) in motif II (DEAD-box), which is essential for the binding of cations for enzyme activity (Tanu et al., 2017). Using identical methods, WT and

mutant DDX41 proteins were purified to near homogeneity (Figure S6A). E345A showed no ATP hydrolysis activity (Figure S6B) and no unwinding activity on the 20-bp duplex DNA substrate (Figure S6C).

Because many helicases have strand annealing activity (Wu, 2012), using two complementary single-stranded DNAs (ssDNAs) of 20-, 30-, 40-, and 50-bp forked DNA in the presence or absence of ATP, we found that the DDX41 protein exhibited strong annealing activity in the absence of ATP, particularly on the 30-bp DNA substrate (Figures 3J-3L, S5M, and S5N). Furthermore, in terms of the directionality of annealing activity, we found that DDX41 preferred the 5'-tailed substrate for annealing rather than the 3'-tailed or blunt-end substrates (Figures S5O-S5Q).

### **NLS acetylation regulates DDX41 trafficking from the nucleus to cytoplasm, where it anneals ssDNA to dsDNA and interacts with cGAS**

The subcellular localization of DDX41 is debatable. DDX41 was initially found as a cytosolic protein (Parvatiyar et al., 2012; Zhang et al., 2011), which fits with the idea that DDX41 is a cytoplasmic DNA sensor. However, several subsequent investigations showed that DDX41 was located in the nucleus (Lewinsohn et al., 2016; Kadono et al., 2016). A recent zebrafish model suggests that Ddx41 traffics from the nucleus to the cytoplasm after DNA stimuli (Ma et al., 2018). To address this more carefully, we examined the subcellular localization of endogenous and exogenous DDX41 protein in human cells. Using a DDX41-specific antibody, we found that endogenous DDX41 is predominantly present in the nucleus and traffics to the cytoplasm, specifically in the perinuclear region, after DNA stimulation (Figure S7A).

Nuclear localization signal (NLS) programs predict that DDX41 contains three potential lysine/arginine-rich NLSs in its N termini—6-PERKRART-13, 97-KAEARK-102, and 162-RVRKKY-167—with the first having the highest possibility (Figure 4A). Also, abstract, DDX41's homolog in *Drosophila*, has an NLS in its N termini (1–194 aa) (Abdul-Ghani et al., 2005). Therefore, we generated GFP-tagged full-length DDX41 and truncated DDX41 that lacked the first two NLSs (DNLS, 127–622 aa). In addition, a natural splicing variant of DDX41, starting from M127, may exist in cells and has reduced nuclear localization and increased cytoplasmic localization (Lewinsohn et al., 2016). Transiently expressed in HeLa cells, we found that DDX41 was predominately localized in the nucleus and trafficked to the cytoplasm 4–6 h after DNA transfection; however, the DDX41- NLS was predominantly localized in the cytoplasm regardless of DNA transfection (Figure 4B). Thus, our data suggest that the NLS located at the extreme N terminus plays a critical role in DDX41's nuclear localization.

The acetylation of NLS modulates the subcellular distribution of IFI16 (Li et al., 2012). DDX41 has a similar NLS in terms of its localization and sequence. After treating cells with trichostatin A (TSA), a broad-spectrum histone deacetylase (HDAC) inhibitor, we noted a significant accumulation of cytoplasmic GFP-DDX41 (Figure 4C), suggesting that acetylation is critical for DDX41's cellular distribution. Next, we changed the lysine at position 9 (K9) to arginine (R) or glutamine (Q) to mimic the nonacetylated or acetylated state, respectively, and to nonfunctional alanine (A). The relative nuclear abundances of Q

and A mutants were significantly reduced compared with the R mutant after DNA stimuli (Figures 4D and S7B), indicating that acetylation of K9 regulates the nuclear/cytoplasmic localization of DDX41.

Because DDX41 contains ATP-independent strand-annealing activity, we next investigated its biological importance to cGAS-STING activation. We transfected WT and DDX41<sup>-/-</sup> THP-1 cells with ssDNA dT<sub>70</sub>, or two complementary strands or annealed dsDNA of VACV70 and scrambled sequence random70 (Table S1), then collected media 6 h post transfection and detected *IFN-β* and *ISG56* gene expression by qPCR, *IFN-β* expression by ELISA assays, and luciferase activity. Compared with a no DNA control, we found that dsDNA had the highest and dT<sub>70</sub> the lowest *IFN-β*, *ISG56*, and luciferase expressions. Strikingly, co-transfection of two complementary oligonucleotides (VACV and scrambled sequences) also induced cytokine responses, with WT cells having much higher responses than DDX41<sup>-/-</sup> cells (Figures 4E-4H). Because DDX41 protein binds ssDNA (Figures S5G and S5R) and anneals two complementary strands (Figures 3K, S5M-S5P, and S5T), we asked whether adding exogenous HSV-1 DNA, such as HSV-1 genome-derived ssDNA, would trigger increased innate response in the presence of DDX41. To this end, we co-infected WT and DDX41<sup>-/-</sup> THP-1 cells with HSV-1 and three doses of HSV-1 30-mer derived from the HSV-1 genome (Table S1) and found increased luciferase production with increasing amounts of HSV-1 30-mer (Figure 4I). Collectively, our findings suggest that DDX41 can anneal the complementary oligonucleotides and form a stable dsDNA that activates cGAS.

To visualize the strand-annealing activity of DDX41, we transfected WT and DDX41<sup>-/-</sup> cells with two complementary oligonucleotides—Cy5-labeled sense (45-mer) and Cy3-labeled antisense (30-mer)—that are, respectively, derived from the VACV 70-mer and its complementary strand (Table S1), which can be bound, unwound, and rewound by the DDX41 protein *in vitro* (Figures S5R-S5T). Interestingly, we observed the co-localization of sense and antisense oligonucleotides in the cytosol after 4 h transfection in WT cells but less in DDX41<sup>-/-</sup> cells (Figure 4J). However, reduced co-localization and extreme instability occurred for the two non-complementary oligonucleotides, random sequence strand (Cy5) and the Cy3-labeled antisense (Table S1), in WT and DDX41<sup>-/-</sup> cells (Figure 4K). Notably, no signal for the two non-complementary oligonucleotides was observed at 4 h post transfection, indicating that non-complementary ssDNAs are unstable due to nuclease attack inside cells. Furthermore, we transfected THP-1 cells with FAM-labeled VACV-70-mer ssDNA and dsDNA. Surprisingly, we found that DDX41 transported from the nucleus to the cytosol and co-localized with VACV-70-mer dsDNA, but not with VACV-70-mer ssDNA (limited signal due to instability), after 4 h of stimulation (Figure 4L). Similar results were obtained using BMDMs and BMDCs (Figure S8).

Furthermore, subcellular fractionation revealed that DDX41 levels increased in the cytosol after 4 h of VACV-70-mer dsDNA or ssDNA stimulation (Figure 4M). Notably, higher DDX41 was observed in dsDNA-stimulated cells than in ssDNA-stimulated cells. Next, we asked whether DDX41 and cGAS have mutual interactions after stimulating with DNA. To this end, we immunoprecipitated the endogenous DDX41 with a cGAS antibody from THP-1 macrophages that were challenged with and without VACV-70-mer dsDNA and

ssDNA. We found a significant pull down of DDX41 by cGAS in dsDNA-stimulated cells compared with ssDNA- or non-stimulated cells (Figure 4N). Visually, we also found that DDX41 co-localized with cGAS after dsDNA transfection, but less after ssDNA transfection, in THP-1 macrophages and mouse primary cells (Figures 4O). To determine whether DDX41 interacts with DNA directly, we performed proximity ligation assays (PLAs) in THP-1 cells. We found that DDX41 interacted with dsDNA (21 PLA signals/cell on average; Figure 4P), ssDNA (7 PLA signals/cell on average; Figure 4Q), and a DNA:RNA hybrid (12 PLA signal/cell on average; Figure 4R). In addition, we labeled HSV-1 genomic DNA with 5-bromo-2'-deoxyuridine (BrdU) during its propagation, and confocal microscopy revealed that DDX41 colocalized with BrdU-labeled viral DNA following HSV-1 infection in HeLa cells (Figure 4S). Moreover, to confirm that DDX41 interacts with invading DNA in the cytoplasm, we performed cross-linking immunoprecipitation (CLIP), for which the DDX41 antibody was used to pull down its associated complex from the cytosolic fractions of THP-1 macrophages; dot blot and PCR assays revealed that the DDX41 antibody, but not the immunoglobulin G (IgG) control, can pull down DNA, including dsDNA, ssDNA, DNA:RNA hybrid, HSV-1 DNA, and oligonucleotides (Figure S9). Since formaldehyde was used in this CLIP experiment, we could not exclude the possibility that DDX41 contacts the tested DNAs through one or more intermediary proteins. However, these findings are consistent with previous reports that DDX41 directly binds DNA (Zhang et al., 2011; Lee et al., 2015).

### **Patient mutant R525H has reduced unwinding activity, retains normal strand-annealing activity, and leads to higher cGAS activity than WT *in vitro***

The c.G1574A (p.R525H) mutation is the most frequent germline and somatic mutation in DDX41 in MDS/AML (Kadono et al., 2016; Polprasert et al., 2015; Quesada et al., 2019; Yoneyama-Hirozane et al., 2017). The residue arginine is highly conserved in DDX41 proteins across species (Figure S10A). To determine its molecular pathogenesis, we generated an R525H mutation and purified the proteins (Figure 5A). The secondary structure prediction by circular dichroism (CD) spectroscopy (Figure 5B) revealed that both WT and R525H proteins feature 39%  $\alpha$ -helix, 20%  $\beta$ -sheet, and 41% unordered structures. After establishing that the mutant R525H protein folded properly, we characterized its DNA-unwinding activity. Using a 30-bp fork-duplex DNA substrate, we observed that R525H had reduced unwinding activity compared with WT DDX41 (Figures 5C and 5D). By increasing the length of the dsDNA from 30 to 40 and 50 bp, we found that the mutant R525H could not unwind the duplex DNA efficiently compared with WT (Figures S10B and S10C). Notably, the R525H protein had a strong band shift, even treated with proteinase K, suggesting that the R525H bound and multimerized on DNA substrates. Because DDX41 has ATP-independent strand-annealing activity (Figures 3J-3L, S6H-L, and S6O), we next performed annealing assays for the R525H protein. We found that R525H could efficiently rewind ssDNA to form dsDNA in the absence of ATP (Figure 5E). However, multimerization again occurred for the R525H protein in the presence of ATP (Figure 5F), which was also observed in gel shift assays using an ATP analog (Figures 5G and S10D). We then examined ATP-hydrolysis activity, where both WT and R525H displayed ATPase activity with stimulator M13 ssDNA (Figure 5H) and dT<sub>30</sub> but not with tRNA and rU<sub>30</sub> (Figures S10E-S10G). Unlike the WT, the R525H mutant displayed

significantly lower ATPase activity (Figures 5H and 5I). As expected, the E345A mutant exhibited no ATP-hydrolysis activity. Using M13 ssDNA as the effector molecule and ATP concentrations ranging from 0 to 4 mM, we determined that the Michaelis constant ( $K_m$ ) value for DDX41-WT was 200  $\mu$ M. We also determined that the  $k_{cat}$  (catalytic rate constants) values for WT and R525H proteins were  $953.6 \pm 45.5$  and  $292.8 \pm 23.6/s$ , respectively. These results suggest that the mutant R525H compromises the ability of DDX41 to hydrolyze ATP.

Because R525H has reduced ATP-hydrolysis activity, we next asked whether R525H could bind ATP. We performed filter-binding assays of DDX41 proteins with [ $\gamma$ - $^{32}$ P] ATP; unexpectedly, we found that R525H had a higher affinity for ATP than WT protein, particularly at a concentration of 150 nM (Figure 5J). Furthermore, we used an ATP AffiPur kit (AK-102, Jena Bioscience), in which we incubated the same amount of WT or R525H proteins with ATP agarose. R525H proteins bound ATP-agarose beads more strongly compared with WT (Figure 5K). Hence, this strong affinity of R525H toward ATP could be a reason for the inefficient/compromised hydrolysis of ATP.

To further assess the consequence of R525H on cGAS activation, we purified human cGAS protein (Figures S11A-S11G). We observed robust cGAS catalytic activity in the presence of dsDNA, particularly tailed dsDNA, but not ssRNA or dT<sub>45</sub> (Figure S11H). In the presence of vaccinia virus dsDNA, cGAS activity increased with increasing DDX41 protein used (Figure 5L). Moreover, cGAMP formation was increased in the presence of the DDX41-R525H or the DDX41-E345A protein and was completely abolished in the presence of the DDX43-WT but not the DDX43-D396A protein (Figure 5M). We believe that cGAS activity was modulated by the dsDNA substrates, which are formed by the DDX41-R525H protein, because of its solo annealing activity and was reduced by the DDX43-WT protein that contains unwinding activity and no strand-annealing activity (Tanu et al., 2017; Yadav et al., 2020).

### Cells expressing R525H have higher type I IFN production

Because R525H has reduced ATP hydrolysis and unwinding activity *in vitro*, we next asked whether overexpression of the DDX41 R525H protein in DDX41-KO cells would rescue the type I IFN production in DDX41 KO cells. Thus, we overexpressed the FLAG-tagged DDX41 proteins (WT or R525H mutant) in DDX41-depleted THP-1 cells (Figure 6A). As expected, overexpression of WT DDX41 rescued type I IFN production in DDX41 KO cells. Unexpectedly, the R525H mutant had higher IFN- $\beta$  production than WT (Figure 6B). Moreover, cGAS oligomerization (Figure 6C), higher cGAMP production (Figure 6D), STING dimerization (Figure 6E), and higher luciferase activity (Figure 6F) occurred in R525H-expressing cells compared with WT-expressing cells. Similar results were obtained in a DDX41 KO HeLa cell line that was reconstituted with DDX41-WT or -R525H (Figure S12).

Given that R525H is the most frequent somatic heterozygous mutation in MDS and AML syndromes (Yoneyama-Hirozane et al., 2017; Lewinsohn et al., 2016; Polprasert et al., 2015), we asked whether it exerts a dominant-negative effect to cause the diseases. To address this, we overexpressed DDX41 (WT or R525H) in THP-1 WT cells (Figure 6G). In



activates cGAS and turns on the cGAS-STING-TBK1-IRF3-type I IFN pathway. On the other hand, DDX41 uses its unwinding activity to separate dsDNA into ssDNA, which turns off the cGAS-STING-TBK1-IRF3-type I IFN pathway. Consistent with our model, a very recent work suggests that DDX41 resolves R loops that regulates the cGAS-STING inflammatory pathway (Weinreb et al., 2021; Mosler et al., 2021). IFI16 negatively regulates cGAS activation through competitive binding agonist DNA (Zheng et al., 2020); therefore, it remains to be determined how DDX41 and IFI16 co-regulate cGAS activation.

DDX41 is a multifunctional protein. The best-known function of DDX41 is mRNA splicing. DDX41 was found in the spliceosomal C complex of HeLa nuclear extract (Jurica et al., 2002; Bessonov et al., 2008). Spliceosomal proteins (e.g., PRPF8 and SF3B1) are top candidates that are pulled down by the V5-tagged DDX41 protein overexpressed in HEK293 cells. Indeed, RNA sequencing (RNA-seq) of DDX41-mutated patient samples show global splicing defects, such as exon skipping and retention (Polprasert et al., 2015). Similar results are found in DDX41's ortholog, *sacy-1*, in *C. elegans* (Tsukamoto et al., 2020). We found that DDX41 takes part in pre-rRNA processing (Kadono et al., 2016). A very recent work on the DDX41 mouse model shows that DDX41 regulates small nucleolar RNA (snoRNA) processing and that DDX41 mutations or loss cause ribosome defects and reduced protein synthesis (Chlon et al., 2021). Notably, DEAD-box proteins are traditionally known for their roles in RNA metabolism (Linder and Jankowsky, 2011); however, several DEAD-box proteins are involved in DNA metabolism, for example, DDX3 (Garbelli et al., 2011), p68 (DDX5) (Tuteja et al., 2014), DDX43 (Tanu et al., 2017), and Dbp9p (DDX56) (Kikuma et al., 2004). Recently, DDX41 in zebrafish was reported to be a crucial gatekeeper of over-producing hematopoietic stem and progenitor cells by inhibiting excessive R loops and thus preventing an inflammatory cascade (Weinreb et al., 2021), suggesting that the DDX41/R-loop/cGAS-STING axis might be driving human hematopoietic malignancy. Notably, DDX41 being an R-loop resolver was confirmed by the R-loop proximity proteomics approach very recently (Mosler et al., 2021). Although DDX41's role as a DNA sensor in innate immunity is well established (Jiang et al., 2017; Andreou, 2021; Omura et al., 2016), we could not exclude the possibility that the impaired innate immune responses we observed in DDX41 KO cells might be a combined consequence of dysregulated mRNA splicing, the cGAS-STING pathway, and/or other factors.

A fundamental question remains unanswered: how are the unwinding and rewinding activities of DDX41 regulated in host cells? We supposed that molecules such as ATP, GTP, and cGAMP would affect DDX41's dual activities. However, no significant effect was observed in our biochemical assays (Figures S5U-S5W). In addition, we obtained K9R and K9Q proteins that mimic the nonacetylated and acetylated states of DDX41, respectively (Figure S6D). Again, no significant effect was observed in our biochemical assays (Figures S6E and S6F). Importantly, separating unwinding and annealing activity is almost impossible when these two activities reside on the same polypeptide (Wu, 2012). We observed that the expression of DDX41 changes throughout DNA infection, specifically increasing 2 h post DNA infection and decreasing 6–12 h after DNA infection (Figures 1D and 1O); however, the strand-annealing activity of DDX41 only occurs at high protein concentrations (Figures 3D, S5M-S5P, and S5T), indicating that it might dominate over unwinding activity when the DDX41 protein reaches high concentrations following viral

infection, then unwinding activity dominates over annealing activity at low concentrations once the virus is cleared. Consistent with DDX41, several helicases, including BLM (Cheok et al., 2005), RECQ5 $\beta$  (Garcia et al., 2004), and LAF-1(DDX3X) (Kim and Myong, 2016), promote strand-annealing activity at high protein concentrations. The DDX41 protein is reported to be degraded through ubiquitination (Zhang et al., 2013), and HSV-1-encoded miR-H2-3p inhibits the expression of DDX41 (Duan et al., 2019), suggesting that the expression of DDX41 might be regulated and therefore, consequently, so is the activity of cGAS (Figure 6N). Intriguingly, patients with MDS who have lower DDX41 expression levels have a significantly increased percentage of bone marrow blasts and a significantly reduced expected survival (Weinreb et al., 2021), suggesting that DDX41 expression levels correlate with clinical outcomes. Therefore, further study is required to determine how the expression of DDX41 is regulated and how the unwinding and rewinding activities of DDX41 are fine-tuned by host cells and/or invading DNA viruses.

Targeting cGAS and/or STING for drug development has been and will continue to be attempted (Haag et al., 2018; Lama et al., 2019). Because it functions upstream of cGAS and STING, DDX41 becomes an important drug target for autoimmune diseases and cancers. Intriguingly, patients with MDS/AML harboring R525H commonly exhibit peripheral blood cytopenias and low blast counts (Yoneyama-Hirozane et al., 2017; Lewinsohn et al., 2016; Polprasert et al., 2015), suggesting that the mutation inhibits the growth and differentiation of hematopoietic cells. Whether higher cytokine responses cause these phenotypes remains unknown; however, chronic innate immune-pathway activation is known to increase the risk of developing myeloid malignancies (Kristinsson et al., 2011), including MDS and AML (Ganan-Gomez et al., 2015; Smith et al., 2019). Thus, DDX41 might play an important role in tumorigenesis and, therefore, developing DDX41 inhibitors will potentially serve as an anticancer strategy.

### Limitations of the study

First, we attempted to monitor the dynamics of dsDNA and ssDNA in WT and DDX41-KO cells. We found that the stability of dsDNA was prolonged in DDX41-KO cells compared with WT cells when we transfected HeLa cells with annealed dsDNA (Figures S13A and S13B). Unfortunately, we barely observed an ssDNA signal when transfecting cells with ssDNA (Figures S13C-S1E), even when using oligonucleotides incorporated with phosphorothioate bonds to prevent nuclease degradation (Table S1). To visualize that DDX41 directly unwinds/anneals DNA in cells, single-molecule-based super-resolution microscopy (Kaniecki et al., 2018) would be used, where DNA will be labeled with fluorescent dyes and DDX41 tagged with GFP or detected by antibody. Second, we attempted to determine which domain of DDX41 controls its strand-annealing activity *in vitro*; however, we have not succeeded. Despite that it has been reported that strand-annealing activity is located or controlled by the C terminus in RecQ5 (Garcia et al., 2004), the N-terminal region in BLM (Chen and Brill, 2010), and the winged-helix domain in RECQ1 (Mukhopadhyay et al., 2021). In addition, we tested c-di-AMP, c-di-GMP, and the cGAS product cGAMP in unwinding and annealing reactions. However, we found that they neither stimulate nor inhibit DDX41's unwinding or annealing activity. Third, we found that DDX41 interacted directly with DNA, including dsDNA and ssDNA; however, we

do not know how DDX41 distinguishes between host cells' own DNA and the DNA of invading pathogens. Despite these limitations, our results identify that DDX41 is required for cGAS-STING activation upon DNA virus infection, probably through modulating the homeostasis of dsDNA and ssDNA.

## STAR★METHODS

### RESOURCE AVAILABILITY

**Lead contact**—Further information and requests for resources and reagents should be directed to the lead contact, Yuliang Wu (yuliang.wu@usask.ca).

**Materials availability**—Plasmids generated in this study will be deposited to Addgene.

DDX41-flp mice (C57BL/6N) were constructed by TaconicArtemis GmbH and obtained from Baylor Research Institute (Baylor Scott & White Research Institute).

### Data and code availability

- Original Western blot images have been deposited at Mendeley Data (<https://doi.org/10.17632/4m9d4xs83j.1>). Microscopy data reported in this paper will be shared by the lead contact upon request.
- This paper does not report original code.
- Any additional information required to reanalyze the data reported in this paper is available from the lead contact upon request.

### EXPERIMENTAL MODEL AND SUBJECT DETAILS

**Cell lines**—HeLa, HEK293T, and Vero cells were grown in Dulbecco's modified Eagle medium (DMEM) supplemented with 10% fetal bovine serum (FBS) (Sigma) and penicillin/streptomycin (100 U/mL each, Sigma). THP-1 cells were cultured in RPMI containing 5% FBS (Sigma), 0.2 mg/mL glutamine (Sigma), 100 U/mL penicillin (Thermo Fisher), 100 µg/mL streptomycin (Thermo Fisher), 10 µg/mL gentamicin sulfate (Lonza), 50 µM β-mercaptoethanol (EMD Biosciences), and 20 mM HEPES (Thermo Fisher). THP-1 WT (thpdnfs) and THP-1 cGAS<sup>-/-</sup> cells (thpd-kocgas) were obtained from InvivoGen. THP-1 cells were differentiated to macrophages with PMA (phorbol 12-myristate 13-acetate, P8139, Sigma, 125 nM for 24 h)

**Mice**—CD11cCre and LyCre Ddx41 conditional KO mice have been previously described (Stavrou et al., 2018; Ma et al., 2022). Both male and female mice were used for experiments. All mice were housed according to the policies of the Animal Care Committee (ACC) of the University of Illinois at Chicago (UIC); all studies were performed following the recommendations in the Guide for the Care and Use of Laboratory Animals of the National Institutes of Health. The experiments performed with mice in this study were approved by the UIC ACC (protocol no. 15–222).

Bone marrow (BM) was isolated from hind limbs of 10- to 12-week-old LyCre-DDX41, CD11cCre-DDX41, and C57BL/6 mice as described (Stavrou et al., 2018). BMs were cultured in DMEM supplemented with 10% FBS, 10 ng/mL macrophage colony stimulating factor (Invitrogen), 1 mM sodium pyruvate, 100 U/mL penicillin, and 100 µg/mL streptomycin, and were harvested 7 d after plating and seeded in 6-well plates for infection assays. BMDCs were cultured in RPMI supplemented with 5% FBS and differentiated with recombinant murine granulocyte-macrophage colony-stimulating factor (20 ng/mL, Invitrogen). Both procedures result in cultures that are ~80–85% pure.

**Patient samples**—Bone marrow aspirates were collected from 23 patients with AML or MDS who participated in the study according to the protocol approved by the ethics committee on human genome research at Hiroshima University. The protocol included the use of pooled samples at initial diagnosis. RNA-seq and gene set enrichment analysis (GSEA) were performed as described previously (Kadono et al., 2016).

**Herpes simplex virus and influenza A virus**—HSV-1 stock (KOS strain) was propagated in Vero cells. For infection of THP-1 cells, the HSV-1 stock was diluted in RPMI and cells were infected at a multiplicity of infection (MOI) of 10 PFU/cell. Titration of serially diluted HSV-1 was performed in Vero cells overlaid with anti-HSV serum. After incubation for 48 h following infection, cells were stained with 0.5% crystal violet in 80% methanol and plaques were counted. Influenza A/PR/8/34 (H1N1) was propagated in 11-day-old embryonated chicken eggs, and virus titers were determined by plaque assays on MDCK cells. The WT and DDX41<sup>-/-</sup> THP-1 cells were mock-infected or infected with IAV at MOI values of 0.1, 1, and 10.

**Co-localization of DDX41 and BrdU-labelled HSV-1 DNA**—To generate BrdU-labeled infectious HSV-1, HSV-1 virus was propagated in Vero cells in media containing BrdU (10 µM, B5002, Sigma). At 24 hpi, BrdU (10 µM) was added once again. To avoid photolysis of BrdU residues, plates were maintained in the dark during the incubation. After 3–4 days, when complete cytopathic effect is reached, the viruses were harvested and purified as following. Dead cells were removed from cell culture supernatant by centrifugation at 1200 rpm for 5 min at 4°C, virus was isolated by centrifuging the supernatant at 17,000×g for 2 h at 4°C, and pellets were resuspended in serum free DMEM/20% glycerol and stored in –80°C. The viral titration was determined by plaque assays. HeLa cells were seeded one day before the infection, and were washed with PBS and then incubated with BrdU labeled HSV-1 (MOI = 10) for 1 h in serum free DMEM at 37°C. After that, cells were incubated in DMEM complete medium until 6 hpi. The cells were fixed with 4% paraformaldehyde for 10 min, washed with PBS, and treated with 4 N HCl for 10 min at room temperature (to expose the BrdU residues for staining). Cells were washed three times with PBS, permeabilized with 0.1% Triton X-100 for 20 min and blocked with 5% BSA in PBS for 1 h at 37°C. Cells were then stained with mouse DDX41 antibody (1:250, Santa Cruz) and rabbit BrdU antibody (1:250, Abcam), followed by detection with fluorescent dye-conjugated secondary antibodies.

**Proximity ligation assay (PLA)**—DDX41-DNA interaction was assessed via proximity ligation assay (PLA) using the Duolink In Situ Red Starter Kit Mouse/Rabbit (DUO92101, Sigma) according to manufacturer's instructions. In brief, THP-1 macrophages were fixed with 100% methanol at  $-20^{\circ}\text{C}$  for 20 min and permeabilized with 100% acetone for 10 min. After washing with Wash Buffer A followed by blocking with Duolink Blocking Buffer for 1 h at  $37^{\circ}\text{C}$  in a humidified chamber, cells were incubated with primary antibodies (DDX41, 1:250, NEB; and dsDNA, 1:250, Abcam or ssDNA, 1:250, US Biological) overnight at  $4^{\circ}\text{C}$ . The next day, cells were washed with Wash Buffer A, followed by incubation with appropriate Duolink secondary antibodies (Sigma) for 1 h in humidity at  $37^{\circ}\text{C}$ . After washing with Wash Buffer A at room temperature, ligation and amplification steps of the PLA were performed according to the manufacturer's protocol. After final washes with Wash Buffer B at room temperature, slides were mounted with Prolong Diamond antifade reagent containing DAPI (Invitrogen). The slides were analyzed and imaged under a confocal microscope; here, red fluorescent dots indicate the close proximity of DNA and DDX41 protein.

**IRF luciferase activity assays**—THP-1-dual reporter cells (InvivoGen) were stably integrated with two inducible reporter constructs, allowing the activation of the NF- $\kappa$ B or IRF pathways to be detected via measurement of secreted alkaline phosphatase or luciferase activity, respectively. At different time points post poly (dA:dT), poly I:C (4  $\mu\text{g}/\text{mL}$ ), or virus stimulation, 20  $\mu\text{L}$  aliquots of media were sampled into 96-well plates. One hundred  $\mu\text{L}$  of Quanti-Luc luciferase substrate (InvivoGen) were added to each well, and plates were read immediately for luciferase activity using a GloMax 96 Microplate Luminometer (Promega).

**Cross-linking immunoprecipitation (CLIP)**—Formaldehyde was added to the media in dropwise to a final concentration of 0.75% (400  $\mu\text{L}$  of 37.7% formaldehyde for 20 mL media) and rotated gently at room temperature for 10 min. Glycine was added to the media to a final concentration of 125 mM (2 mL of 1.25 M glycine for 20 mL media) and incubated with shaking for 5 min at room temperature. Cells were washed with PBS and proceeded to the steps as regular IP.

**RT-qPCR**—Total RNA was extracted from cells using Trizol reagent (Invitrogen) and reverse-transcribed to cDNA using Superscript II Reverse Transcriptase and oligo-dT primer (Invitrogen). The expression of various mRNAs was measured by quantitative real-time PCR using gene-specific primers and SYBR green master mix (A25742, Applied Biosciences). Relative expression was calculated using glyceraldehyde-3-phosphate dehydrogenase (GAPDH) as a reference gene. Samples were analyzed in triplicate per reaction using the StepOnePlus Real-Time PCR System (Applied Biosystems).

**Biochemical assays of DDX41 protein**—Helicase assays, strand annealing assays, electrophoretic mobility shift assays (EMSA), and ATP hydrolysis assays for DDX41 protein were performed as described for DDX43 helicase and other helicases (Tanu et al., 2017; Yadav et al., 2020; Guo et al., 2016; Singh et al., 2022).

***In vitro* cGAMP synthesis assays**—cGAMP synthesis assays were performed in buffer containing 20 mM Tris (pH 7.5), 150 mM NaCl, 1 mM DTT, and 10 mM MgCl<sub>2</sub>. Reactions (20 μL) were initiated with 2.5 μM of DDX41 or DDX43 protein, nucleic acids (1 μM), and cGAS protein (2.5 μM) in the presence of cold ATP and GTP (250 μM each) and [ $\alpha$ -<sup>32</sup>P] ATP (10 μCi, PerkinElmer). The reactions were incubated at 37°C for 1.5 h and terminated with the addition of 5 U of shrimp alkaline phosphatase (NEB) at 37°C for 30 min to digest the remaining labeled nucleoside triphosphates, followed by heating at 65°C for 20 min. One μL of each reaction was spotted onto a PEI-cellulose TLC plate (J.T. Baker) and separated with 1.5 M KH<sub>2</sub>PO<sub>4</sub> (pH 3.8) as the solvent. Radiolabeled products were detected with a phosphor screen using a Typhoon FLA 7000.

## QUANTIFICATION AND STATISTICAL ANALYSIS

All statistical analyses were performed in GraphPad Prism 8 or Microsoft Excel. Analyses of relative gene expression were determined using the  $2^{-Ct}$  method with GAPDH as the internal reference gene. Results are reported as mean  $\pm$  SEM of at least three independent experiments. Comparisons were analyzed using an unpaired Student's t-test or one-way analysis of variance (ANOVA) with multiple comparison were performed with Tukey's multiple comparison test (NS:  $p > 0.05$ , \* $p < 0.05$ , \*\* $p < 0.01$ , \*\*\* $p < 0.001$ , and \*\*\*\* $p < 0.0001$ ), as indicated in the individual figures.

## Supplementary Material

Refer to Web version on PubMed Central for supplementary material.

## ACKNOWLEDGMENTS

The authors thank Michael Seidman (NIA-NIH) for useful discussions. This work was supported by grants from the Natural Sciences and Engineering Research Council of Canada (NSERC, RGPIN 2019-04578) to Y.Z.; the Canada Foundation for Innovation (CFI-33364) and Cancer Research Society (CRS-22493) to F.J.V.; the National Institutes of Health (R01-AI-085015) to S.R.R.; and the NSERC (RGPIN-2019-05487), the Canadian Cancer Society (CBCF-R1636), the Cancer Research Society (CRS-24139), and the Saskatchewan Health Research Foundation (SHRF-5093) to Y.W.

## REFERENCES

- Abdul-Ghani M, Hartman KL, and Ngsee JK (2005). Abstrakt interacts with and regulates the expression of sorting nexin-2. *J. Cell Physiol* 204, 210–218. [PubMed: 15690390]
- Abe T, Harashima A, Xia T, Konno H, Konno K, Morales A, Ahn J, Gutman D, and Barber GN (2013). STING recognition of cytoplasmic DNA instigates cellular defense. *Mol. Cell* 50, 5–15. [PubMed: 23478444]
- Ablasser A, Bauernfeind F, Hartmann G, Latz E, Fitzgerald KA, and Hornung V (2009). RIG-I-dependent sensing of poly(dA:dT) through the induction of an RNA polymerase III-transcribed RNA intermediate. *Nat. Immunol* 10, 1065–1072. [PubMed: 19609254]
- Ablasser A, and Chen ZJ (2019). cGAS in action: expanding roles in immunity and inflammation. *Science* 363, eaat8657. [PubMed: 30846571]
- Abou Dalle I, Kantarjian H, Bannon SA, Kanagal-Shamanna R, Routbort M, Patel KP, Hu S, Bhalla K, Garcia-Manero G, and Dinardo CD (2019). Successful lenalidomide treatment in high risk myelodysplastic syndrome with germline DDX41 mutation. *Am. J. Hematol* 95, 227–229. [PubMed: 31400013]
- Akira S, Uematsu S, and Takeuchi O (2006). Pathogen recognition and innate immunity. *Cell* 124, 783–801. [PubMed: 16497588]

- Alkhateeb HB, Nanaa A, Viswanatha DS, Foran JM, Badar T, Sproat L, He R, Nguyen P, Jevremovic D, Salama ME, et al. (2021). Genetic features and clinical outcomes of patients with isolated and comutated DDX41-mutated myeloid neoplasms. *Blood Adv.* 6, 528–532.
- Andreou AZ (2021). DDX41: a multifunctional DEAD-box protein involved in pre-mRNA splicing and innate immunity. *Biol. Chem* 402, 645–651. [PubMed: 33711218]
- Bannon SA, Routbort MJ, Montalban-Bravo G, Mehta RS, Jelloul FZ, Takahashi K, Daver N, Oran B, Pemmaraju N, Borthakur G, et al. (2020). Next-generation sequencing of DDX41 in myeloid neoplasms leads to increased detection of germline alterations. *Front Oncol.* 10, 582213. [PubMed: 33585199]
- Benmerzoug S, Rose S, Bounab B, Gosset D, Duneau L, Chenuet P, Mollet L, Le Bert M, Lambers C, Geleff S, et al. (2018). STING-dependent sensing of self-DNA drives silica-induced lung inflammation. *Nat. Commun* 9, 5226. [PubMed: 30523277]
- Bessonov S, Anokhina M, Will CL, Urlaub H, and Luhrmann R (2008). Isolation of an active step I spliceosome and composition of its RNP core. *Nature* 452, 846–850. [PubMed: 18322460]
- Boyer JA, Spangler CJ, Strauss JD, Cesmat AP, Liu P, Mcginty RK, and Zhang Q (2020). Structural basis of nucleosome-dependent cGAS inhibition. *Science* 370, 450–454. [PubMed: 32913000]
- Cao D, Han X, Fan X, Xu RM, and Zhang X (2020). Structural basis for nucleosome-mediated inhibition of cGAS activity. *Cell Res.* 30, 1088–1097. [PubMed: 33051594]
- Cardoso S, Ryan G, Walne A, Ellison A, Lowe R, Tummala H, Rio-Machin A, Collopy L, Al Seraihi A, and Wallis Y (2016). Germline heterozygous DDX41 variants in a subset of familial myelodysplasia and acute myeloid leukemia. *Leukemia* 30, 2083–2086. [PubMed: 27133828]
- Chen CF, and Brill SJ (2010). An essential DNA strand-exchange activity is conserved in the divergent N-termini of BLM orthologs. *EMBO J.* 29, 1713–1725. [PubMed: 20389284]
- Chen Q, Sun L, and Chen ZJ (2016). Regulation and function of the cGAS-STING pathway of cytosolic DNA sensing. *Nat. Immunol* 17, 1142–1149. [PubMed: 27648547]
- Cheok CF, Wu L, Garcia PL, Janscak P, and Hickson ID (2005). The Bloom's syndrome helicase promotes the annealing of complementary single-stranded DNA. *Nucleic Acids Res.* 33, 3932–3941. [PubMed: 16024743]
- Chlon TM, Stepanchick E, Hershberger CE, Daniels NJ, Hueneman KM, Kuenzi Davis A, Choi K, Zheng Y, Gurnari C, Haferlach T, et al. (2021). Germline DDX41 mutations cause ineffective hematopoiesis and myelodysplasia. *Cell Stem Cell* 28, 1966–1981. [PubMed: 34473945]
- Choi EJ, Cho YU, Hur EH, Jang S, Kim N, Park HS, Lee JH, Lee KH, Kim SH, Hwang SH, et al. (2021). Unique ethnic features of DDX41 mutations in patients with idiopathic cytopenia of undetermined significance, myelodysplastic syndrome, or acute myeloid leukemia. *Haematologica* 107, 510–518.
- Churpek JE, and Smith-Simmer K (1993). Ddx41-Associated familial myelodysplastic syndrome and acute myeloid leukemia. In *GeneReviews((R))*, M.P. Adam, H.H. Ardinger, R.A. Pagon, S.E. Wallace, L.J.H. Bean, G. Mirzaa, and A. Amemiya, eds. (University of Washington), pp. 1–23.
- Ding L, Ley TJ, Larson DE, Miller CA, Koboldt DC, Welch JS, Ritchey JK, Young MA, Lamprecht T, and McLellan MD (2012). Clonal evolution in relapsed acute myeloid leukaemia revealed by whole-genome sequencing. *Nature* 481, 506–510. [PubMed: 22237025]
- Duan Y, Zeng J, Fan S, Liao Y, Feng M, Wang L, Zhang Y, and Li Q (2019). Herpes simplex virus type 1-encoded miR-H2-3p manipulates cytosolic DNA-stimulated antiviral innate immune response by targeting DDX41. *Viruses* 11, 756.
- Duployez N, Largeaud L, Duchmann M, Kim R, Rieunier J, Lambert J, Bidet A, Larcher L, Lemoine J, Delhommeau F, et al. (2022). Prognostic impact of DDX41 germline mutations in intensively treated acute myeloid leukemia patients: an ALFA-FILO study. *Blood.* blood.2021015328. In press.
- Fazio F, Quintini M, Carosino I, Matteucci C, Miulli E, Pellanera F, Lucani B, Ansuinelli M, Breccia M, Mecucci C, and Latagliata R (2021). New dead/H-box helicase gene (ddx41) mutation in an Italian family with recurrent leukemia. *Leuk. Lymphoma* 62, 1–4. [PubMed: 33356706]
- Ganan-Gomez I, Wei Y, Starczynowski DT, Colla S, Yang H, Cabrero-Calvo M, Bohannan ZS, Verma A, Steidl U, and Garcia-Manero G (2015). Deregulation of innate immune and inflammatory signaling in myelodysplastic syndromes. *Leukemia* 29, 1458–1469. [PubMed: 25761935]

- Garbelli A, Beermann S, Di Cicco G, Dietrich U, and Maga G (2011). A motif unique to the human DEAD-box protein DDX3 is important for nucleic acid binding, ATP hydrolysis, RNA/DNA unwinding and HIV-1 replication. *PLoS One* 6, e19810. [PubMed: 21589879]
- Garcia PL, Liu Y, Jiricny J, West SC, and Janscak P (2004). Human RECQ5beta, a protein with DNA helicase and strand-annealing activities in a single polypeptide. *EMBO J.* 23, 2882–2891. [PubMed: 15241474]
- Goyal T, Tu ZJ, Wang Z, and Cook JR (2021). Clinical and pathologic spectrum of DDX41-mutated hematolymphoid neoplasms. *Am. J. Clin. Pathol* 156, 829–838. [PubMed: 33929502]
- Guo M, Vidhyasagar V, Talwar T, Kariem A, and Wu Y (2016). Mutational analysis of FANCD1 helicase. *Methods* 108, 118–129. [PubMed: 27107905]
- Haag SM, Gulen MF, Reymond L, Gibelin A, Abrami L, Decout A, Heymann M, Van Der Goot FG, Turcatti G, Behrendt R, and Ablasser A (2018). Targeting STING with covalent small-molecule inhibitors. *Nature* 559, 269–273. [PubMed: 29973723]
- Hosono N (2019). [Genetic defects of chromosome 5q and 7q in myeloid neoplasms]. *Rinsho Ketsueki* 60, 800–809. [PubMed: 31391370]
- Hu J, Xu X, Wang S, and Ge G (2020). Ctenopharyngodon idellus DDX41 initiates IFN I and ISG15 expression in response to GCRV infection. *Fish Shellfish Immunol.* 106, 149–160. [PubMed: 32781207]
- Iacobucci I, Wen J, Meggendorfer M, Choi JK, Shi L, Pounds SB, Carmichael CL, Masih KE, Morris SM, Lindsley RC, et al. (2019). Genomic subtyping and therapeutic targeting of acute erythroleukemia. *Nat. Genet* 51, 694–704. [PubMed: 30926971]
- Irion U, and Leptin M (1999). Developmental and cell biological functions of the Drosophila DEAD-box protein abstract. *Curr. Biol* 9, 1373–1381. [PubMed: 10607561]
- Jiang Y, Zhu Y, Liu ZJ, and Ouyang S (2017). The emerging roles of the DDX41 protein in immunity and diseases. *Protein Cell* 8, 83–89. [PubMed: 27502187]
- Jin L, Hill KK, Filak H, Mogan J, Knowles H, Zhang B, Perraud AL, Cambier JC, and Lenz LL (2011). MPYS is required for IFN response factor 3 activation and type I IFN production in the response of cultured phagocytes to bacterial second messengers cyclic-di-AMP and cyclic-di-GMP. *J. Immunol* 187, 2595–2601. [PubMed: 21813776]
- Jurica MS, Licklider LJ, Gygi SR, Grigorieff N, and Moore MJ (2002). Purification and characterization of native spliceosomes suitable for three-dimensional structural analysis. *RNA* 8, 426–439. [PubMed: 11991638]
- Kadono M, Kanai A, Nagamachi A, Shinriki S, Kawata J, Iwato K, Kyo T, Oshima K, Yokoyama A, Kawamura T, et al. (2016). Biological implications of somatic DDX41 p.R525H mutation in acute myeloid leukemia. *Exp. Hematol* 44, 745–754.e4. [PubMed: 27174803]
- Kaniecki K, De Tullio L, and Greene EC (2018). A change of view: homologous recombination at single-molecule resolution. *Nat. Rev. Genet* 19, 191–207. [PubMed: 29225334]
- Kikuma T, Ohtsu M, Utsugi T, Koga S, Okuhara K, Eki T, Fujimori F, and Murakami Y (2004). Dbp9p, a member of the DEAD box protein family, exhibits DNA helicase activity. *J. Biol. Chem* 279, 20692–20698. [PubMed: 15028736]
- Kim B, Yun W, Lee ST, Choi JR, Yoo KH, Koo HH, Jung CW, and Kim SH (2020). Prevalence and clinical implications of germline predisposition gene mutations in patients with acute myeloid leukemia. *Sci. Rep* 10, 14297. [PubMed: 32868804]
- Kim Y, and Myong S (2016). RNA remodeling activity of DEAD box proteins tuned by protein concentration, RNA length, and ATP. *Mol. Cell* 63, 865–876. [PubMed: 27546789]
- Kranzusch PJ, Lee AS, Berger JM, and Doudna JA (2013). Structure of human cGAS reveals a conserved family of second-messenger enzymes in innate immunity. *Cell Rep* 3, 1362–1368. [PubMed: 23707061]
- Kristinsson SY, Bjorkholm M, Hultcrantz M, Derolf AR, Landgren O, and Goldin LR (2011). Chronic immune stimulation might act as a trigger for the development of acute myeloid leukemia or myelodysplastic syndromes. *J. Clin. Oncol* 29, 2897–2903. [PubMed: 21690473]
- Kujirai T, Zierhut C, Takizawa Y, Kim R, Negishi L, Uruma N, Hirai S, Funabiki H, and Kurumizaka H (2020). Structural basis for the inhibition of cGAS by nucleosomes. *Science* 370, 455–458. [PubMed: 32912999]

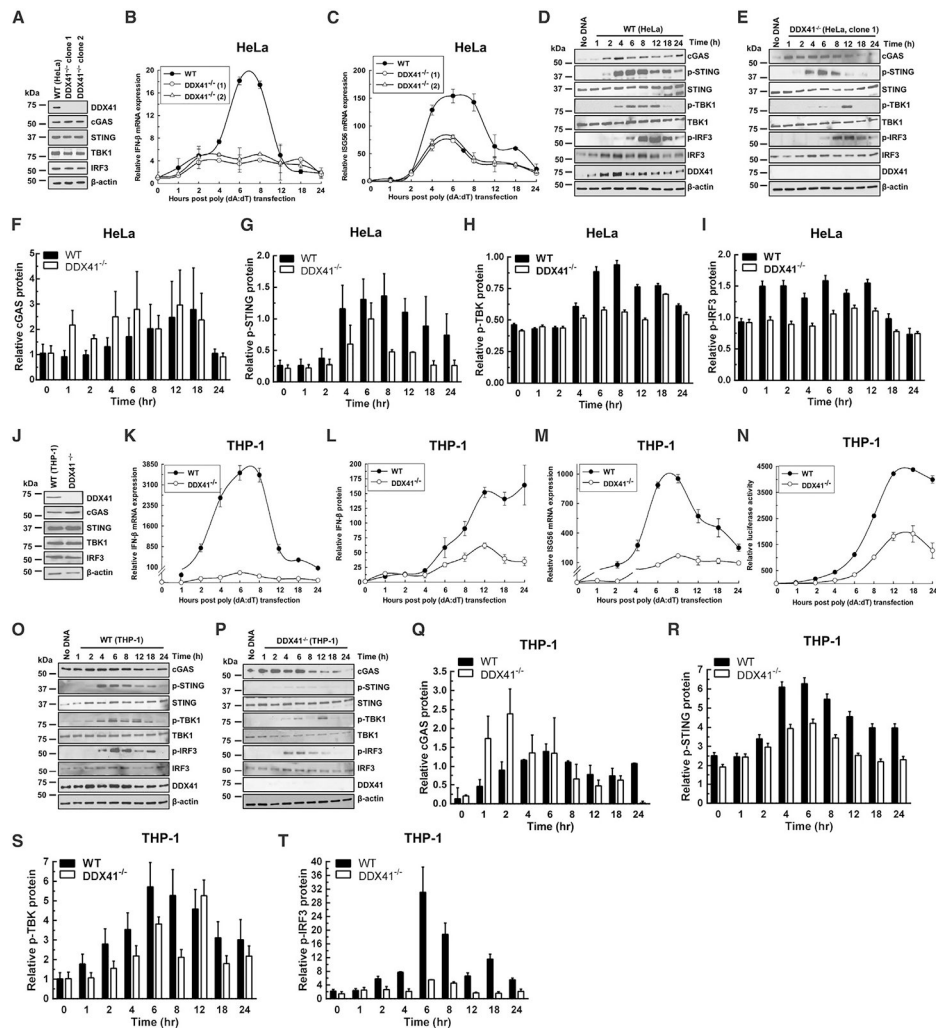
- Lama L, Adura C, Xie W, Tomita D, Kamei T, Kuryavyi V, Gogakos T, Steinberg JI, Miller M, Ramos-Espiritu L, et al. (2019). Development of human cGAS-specific small-molecule inhibitors for repression of dsDNA-triggered interferon expression. *Nat. Commun* 10, 2261. [PubMed: 31113940]
- Lau L, Gray EE, Brunette RL, and Stetson DB (2015). DNA tumor virus oncogenes antagonize the cGAS-STING DNA-sensing pathway. *Science* 350, 568–571. [PubMed: 26405230]
- Lee KG, Kim SS, Kui L, Voon DC, Mauduit M, Bist P, Bi X, Pereira NA, Liu C, Sukumaran B, et al. (2015). Bruton's tyrosine kinase phosphorylates DDX41 and activates its binding of dsDNA and STING to initiate type I interferon response. *Cell Rep* 10, 1055–1065. [PubMed: 25704810]
- Lewinsohn M, Brown AL, Weinel LM, Phung C, Rafidi G, Lee MK, Schreiber AW, Feng J, Babic M, Chong CE, et al. (2016). Novel germ line DDX41 mutations define families with a lower age of MDS/AML onset and lymphoid malignancies. *Blood* 127, 1017–1023. [PubMed: 26712909]
- Li P, White T, Xie W, Cui W, Peker D, Zeng G, Wang HY, Vagher J, Brown S, Williams M, et al. (2021). AML with germline DDX41 variants is a clinicopathologically distinct entity with an indolent clinical course and favorable outcome. *Leukemia* 36, 664–674. [PubMed: 34671111]
- Li R, Sobreira N, Witmer PD, Pratz KW, and Braunstein EM (2016). Two novel germline DDX41 mutations in a family with inherited myelodysplasia/acute myeloid leukemia. *Haematologica* 101, e228–e231. [PubMed: 26944477]
- Li T, Diner BA, Chen J, and Cristea IM (2012). Acetylation modulates cellular distribution and DNA sensing ability of interferon-inducible protein IFI16. *Proc. Natl. Acad. Sci. U S A* 109, 10558–10563. [PubMed: 22691496]
- Li XD, Wu J, Gao D, Wang H, Sun L, and Chen ZJ (2013). Pivotal roles of cGAS-cGAMP signaling in antiviral defense and immune adjuvant effects. *Science* 341, 1390–1394. [PubMed: 23989956]
- Linder P, and Jankowsky E (2011). From unwinding to clamping - the DEAD box RNA helicase family. *Nat. Rev. Mol. Cell Biol* 12, 505–516. [PubMed: 21779027]
- Ma F, Li B, Liu SY, Iyer SS, Yu Y, Wu A, and Cheng G (2015). Positive feedback regulation of type I IFN production by the IFN-inducible DNA sensor cGAS. *J. Immunol* 194, 1545–1554. [PubMed: 25609843]
- Ma J, Mahmud N, Bosland MC, and Ross SR (2022). DDX41 is needed for pre- and postnatal hematopoietic stem cell differentiation in mice. *Stem Cell Rep.* 17, 879–893.
- Ma JX, Li JY, Fan DD, Feng W, Lin AF, Xiang LX, and Shao JZ (2018). Identification of DEAD-box RNA helicase DDX41 as a trafficking protein that involves in multiple innate immune signaling pathways in a zebrafish model. *Front Immunol.* 9, 1327. [PubMed: 29942316]
- Michalski S, De Oliveira Mann CC, Stafford CA, Witte G, Bartho J, Lammens K, Hornung V, and Hopfner KP (2020). Structural basis for sequestration and autoinhibition of cGAS by chromatin. *Nature* 587, 678–682. [PubMed: 32911480]
- Miles AJ, Ramalli SG, and Wallace BA (2022). DichroWeb, a website for calculating protein secondary structure from circular dichroism spectroscopic data. *Protein Sci.* 31, 37–46. [PubMed: 34216059]
- Mosler T, Conte F, Longo GMC, Mikicic I, Kreim N, Mockel MM, Petrosino G, Flach J, Barau J, Luke B, et al. (2021). R-loop proximity proteomics identifies a role of DDX41 in transcription-associated genomic instability. *Nat. Commun* 12, 7314. [PubMed: 34916496]
- Mukhopadhyay S, Das T, Bose M, Jain CK, Chakraborty M, Mukherjee S, Shikha K, Das AK, and Ganguly A (2021). Residues at the interface between zinc binding and winged helix domains of human RECQ1 play a significant role in DNA strand annealing activity. *Nucleic Acids Res.* 49, 11834–11854. [PubMed: 34751402]
- Omura H, Oikawa D, Nakane T, Kato M, Ishii R, Ishitani R, Tokunaga F, and Nureki O (2016). Structural and Functional Analysis of DDX41: a bispecific immune receptor for DNA and cyclic dinucleotide. *Sci. Rep* 6, 34756. [PubMed: 27721487]
- Ouyang S, Song X, Wang Y, Ru H, Shaw N, Jiang Y, Niu F, Zhu Y, Qiu W, Parvatiyar K, et al. (2012). Structural analysis of the STING adaptor protein reveals a hydrophobic dimer interface and mode of cyclic di-GMP binding. *Immunity* 36, 1073–1086. [PubMed: 22579474]
- Parvatiyar K, Zhang Z, Teles RM, Ouyang S, Jiang Y, Iyer SS, Zaver SA, Schenk M, Zeng S, Zhong W, et al. (2012). The helicase DDX41 recognizes the bacterial secondary messengers cyclic

- di-GMP and cyclic di-AMP to activate a type I interferon immune response. *Nat. Immunol* 13, 1155–1161. [PubMed: 23142775]
- Pathare GR, Decout A, Gluck S, Cavadini S, Makasheva K, Hovius R, Kempf G, Weiss J, Kozicka Z, Guey B, et al. (2020). Structural mechanism of cGAS inhibition by the nucleosome. *Nature* 587, 668–672. [PubMed: 32911482]
- Polprasert C, Schulze I, Sekeres MA, Makishima H, Przychodzen B, Hosono N, Singh J, Padgett RA, Gu X, Phillips JG, et al. (2015). Inherited and somatic defects in DDX41 in myeloid neoplasms. *Cancer Cell* 27, 658–670. [PubMed: 25920683]
- Polprasert C, Takeda J, Niparuck P, Rattanathamthee T, Pirunsarn A, Suksusut A, Kobbuaklee S, Wudhikarn K, Lawasut P, Kongkiatkamon S, et al. (2020). Novel DDX41 variants in Thai patients with myeloid neoplasms. *Int. J. Hematol* 111, 241–246. [PubMed: 31713024]
- Pyle AM (2008). Translocation and unwinding mechanisms of RNA and DNA helicases. *Annu. Rev. Biophys* 37, 317–336. [PubMed: 18573084]
- Qu S, Li B, Qin T, Xu Z, Pan L, Hu N, Huang G, Peter Gale R, and Xiao Z (2020). Molecular and clinical features of myeloid neoplasms with somatic DDX41 mutations. *Br. J. Haematol* 192, 1006–1010. [PubMed: 32307695]
- Quesada AE, Routbort MJ, Dinardo CD, Bueso-Ramos CE, Kanagal-Shamanna R, Khoury JD, Thakral B, Zuo Z, Yin CC, Loghavi S, et al. (2019). DDX41 mutations in myeloid neoplasms are associated with male gender, TP53 mutations and high-risk disease. *Am. J. Hematol* 94, 757–766. [PubMed: 30963592]
- Singh RS, Arna AB, Dong H, Yadav M, Aggarwal A, and Wu Y (2022). Structure-function analysis of DEAD-box helicase DDX43. *Methods* S1046-2023, 00068–8.
- Singhal D, Hahn CN, Feurstein S, Wee LYA, Moma L, Kutyna MM, Chhetri R, Eshraghi L, Schreiber AW, Feng J, et al. (2021). Targeted gene panels identify a high frequency of pathogenic germline variants in patients diagnosed with a hematological malignancy and at least one other independent cancer. *Leukemia* 35, 3245–3256. [PubMed: 33850299]
- Smith MA, Choudhary GS, Pellagatti A, Choi K, Bolanos LC, Bhagat TD, Gordon-Mitchell S, Von Ahrens D, Pradhan K, Steeples V, et al. (2019). U2AF1 mutations induce oncogenic IRAK4 isoforms and activate innate immune pathways in myeloid malignancies. *Nat. Cell Biol* 21, 640–650. [PubMed: 31011167]
- Soponpong S, Amparyup P, and Tassanakajon A (2018). A cytosolic sensor, PmDDX41, mediates antiviral immune response in black tiger shrimp *Penaeus monodon*. *Dev. Comp. Immunol* 81, 291–302. [PubMed: 29248385]
- Stavrou S, Aguilera AN, Blouch K, and Ross SR (2018). DDX41 recognizes RNA/DNA retroviral reverse transcripts and is critical for in vivo control of murine leukemia virus infection. *MBio* 9, e00923–18. [PubMed: 29871919]
- Sun H, Huang Y, Mei S, Xu F, Liu X, Zhao F, Yin L, Zhang D, Wei L, Wu C, et al. (2021). A nuclear export signal is required for cGAS to sense cytosolic DNA. *Cell Rep* 34, 108586. [PubMed: 33406424]
- Sun L, Wu J, Du F, Chen X, and Chen ZJ (2013). Cyclic GMP-AMP synthase is a cytosolic DNA sensor that activates the type I interferon pathway. *Science* 339, 786–791. [PubMed: 23258413]
- Takeuchi O, and Akira S (2010). Pattern recognition receptors and inflammation. *Cell* 140, 805–820. [PubMed: 20303872]
- Tanu T, Vidhyasagar V, Qing J, Guo M, Kariem A, Lu Y, Singh RS, Lukong KE, and Wu Y (2017). The DEAD-box protein DDX43 (HAGE) is a dual RNA-DNA helicase and has a K-homology domain required for full nucleic acid unwinding activity. *J. Biol. Chem* 292, 10429–10443. [PubMed: 28468824]
- Theofilopoulos AN, Kono DH, and Baccala R (2017). The multiple pathways to autoimmunity. *Nat. Immunol* 18, 716–724. [PubMed: 28632714]
- Thompson MR, Kaminski JJ, Kurt-Jones EA, and Fitzgerald KA (2011). Pattern recognition receptors and the innate immune response to viral infection. *Viruses* 3, 920–940. [PubMed: 21994762]
- Tsukamoto T, Gearhart MD, Kim S, Mekonnen G, Spike CA, and Greenstein D (2020). Insights into the involvement of spliceosomal mutations in myelodysplastic disorders from analysis of SACY-1/DDX41 in *Caenorhabditis elegans*. *Genetics* 214, 869–893. [PubMed: 32060018]

- Tuteja N, Tarique M, Banu MS, Ahmad M, and Tuteja R (2014). Pisum sativum p68 DEAD-box protein is ATP-dependent RNA helicase and unique bipolar DNA helicase. *Plant Mol. Biol* 85, 639–651. [PubMed: 24908423]
- Unterholzner L, Keating SE, Baran M, Horan KA, Jensen SB, Sharma S, Sirois CM, Jin T, Latz E, Xiao TS, et al. (2010). IFI16 is an innate immune sensor for intracellular DNA. *Nat. Immunol* 11, 997–1004. [PubMed: 20890285]
- Volkman HE, Cambier S, Gray EE, and Stetson DB (2019). Tight nuclear tethering of cGAS is essential for preventing autoreactivity. *Elife* 8, e47491. [PubMed: 31808743]
- Wang Y, Ning X, Gao P, Wu S, Sha M, Lv M, Zhou X, Gao J, Fang R, Meng G, et al. (2017). Inflammasome activation triggers caspase-1-mediated cleavage of cGAS to regulate responses to DNA virus infection. *Immunity* 46, 393–404. [PubMed: 28314590]
- Weinreb JT, Ghazale N, Pradhan K, Gupta V, Potts KS, Tricoli B, Daniels NJ, Padgett RA, De Oliveira S, Verma A, and Bowman TV (2021). Excessive R-loops trigger an inflammatory cascade leading to increased HSPC production. *Dev. Cell* 56, 627–640.e5. [PubMed: 33651979]
- Wu Y (2012). Unwinding and rewinding: double faces of helicase? *J. Nucleic Acids* 2012, 140601. [PubMed: 22888405]
- Xie W, Lama L, Adura C, Tomita D, Glickman JF, Tuschl T, and Patel DJ (2019). Human cGAS catalytic domain has an additional DNA-binding interface that enhances enzymatic activity and liquid-phase condensation. *Proc. Natl. Acad. Sci. U S A* 116, 11946–11955. [PubMed: 31142647]
- Yadav M, Singh RS, Hogan D, Vidhyasagar V, Yang S, Chung IYW, Kusalik A, Dmitriev OY, Cygler M, and Wu Y (2020). The KH domain facilitates the substrate specificity and unwinding processivity of DDX43 helicase. *J. Biol. Chem* 296, 100085. [PubMed: 33199368]
- Yang F, Long N, Anekpuritanang T, Bottomly D, Savage JC, Lee T, Solis-Ruiz JM, Borate U, Wilmot B, Tognon CE, et al. (2021). Identification and prioritization of myeloid malignancy germline variants in a large cohort of adult AML patients. *Blood* 139, 1208–1221.
- Yoneyama-Hirozane M, Kondo M, Matsumoto SI, Morikawa-Oki A, Morishita D, Nakanishi A, Kawamoto T, and Nakayama M (2017). High-throughput screening to identify inhibitors of DEAD box helicase DDX41. *SLAS Discov.* 22, 1084–1092. [PubMed: 28426938]
- Zhang X, Wu J, Du F, Xu H, Sun L, Chen Z, Brautigam CA, Zhang X, and Chen ZJ (2014). The cytosolic DNA sensor cGAS forms an oligomeric complex with DNA and undergoes switch-like conformational changes in the activation loop. *Cell Rep* 6, 421–430. [PubMed: 24462292]
- Zhang Z, Bao M, Lu N, Weng L, Yuan B, and Liu YJ (2013). The E3 ubiquitin ligase TRIM21 negatively regulates the innate immune response to intracellular double-stranded DNA. *Nat. Immunol* 14, 172–178. [PubMed: 23222971]
- Zhang Z, Yuan B, Bao M, Lu N, Kim T, and Liu YJ (2011). The helicase DDX41 senses intracellular DNA mediated by the adaptor STING in dendritic cells. *Nat. Immunol* 12, 959–965. [PubMed: 21892174]
- Zhao B, Xu P, Rowlett CM, Jing T, Shinde O, Lei Y, West AP, Liu WR, and Li P (2020). The molecular basis of tight nuclear tethering and inactivation of cGAS. *Nature* 587, 673–677. [PubMed: 32911481]
- Zheng W, Zhou R, Li S, He S, Luo J, Zhu M, Chen N, Chen H, Meurens F, and Zhu J (2020). Porcine IFI16 negatively regulates cGAS signaling through the restriction of DNA binding and stimulation. *Front Immunol.* 11, 1669. [PubMed: 32922386]
- Zhou W, Whiteley AT, De Oliveira Mann CC, Morehouse BR, Nowak RP, Fischer ES, Gray NS, Mekalanos JJ, and Kranzusch PJ (2018). Structure of the human cGAS-DNA complex reveals enhanced control of immune surveillance. *Cell* 174, 300–311.e11. [PubMed: 30007416]

**Highlights**

- DDX41 is required for cGAS-STING activation
- DDX41 modulates the homeostasis of dsDNA through its unwinding and annealing activities
- Patient mutant R525H has reduced unwinding activity but retains annealing activity
- R525H causes excessive activation of innate immune response that might lead to MDS/AML



(M) qPCR analysis of *ISG56* gene expression in WT and DDX41 KO THP-1 macrophages after poly(dA:dT) treatment.

(N) IRF-induced luciferase activity measured in WT and DDX41 KO THP-1 macrophages after poly(dA:dT) treatment.

(O and P) Western blot assays of proteins in the cGAS-STING pathway in WT (O) and DDX41 KO (P) THP-1 macrophages after poly(dA:dT) treatment.

(Q–T) Quantification of the relative expression of cGAS (Q), p-STING (R), p-TBK1 (S), and p-IRF3 (T).

For (B), (C), (F)–(I), (K)–(N), and (Q)–(T): data represent the mean  $\pm$  SEM of three independent experiments.

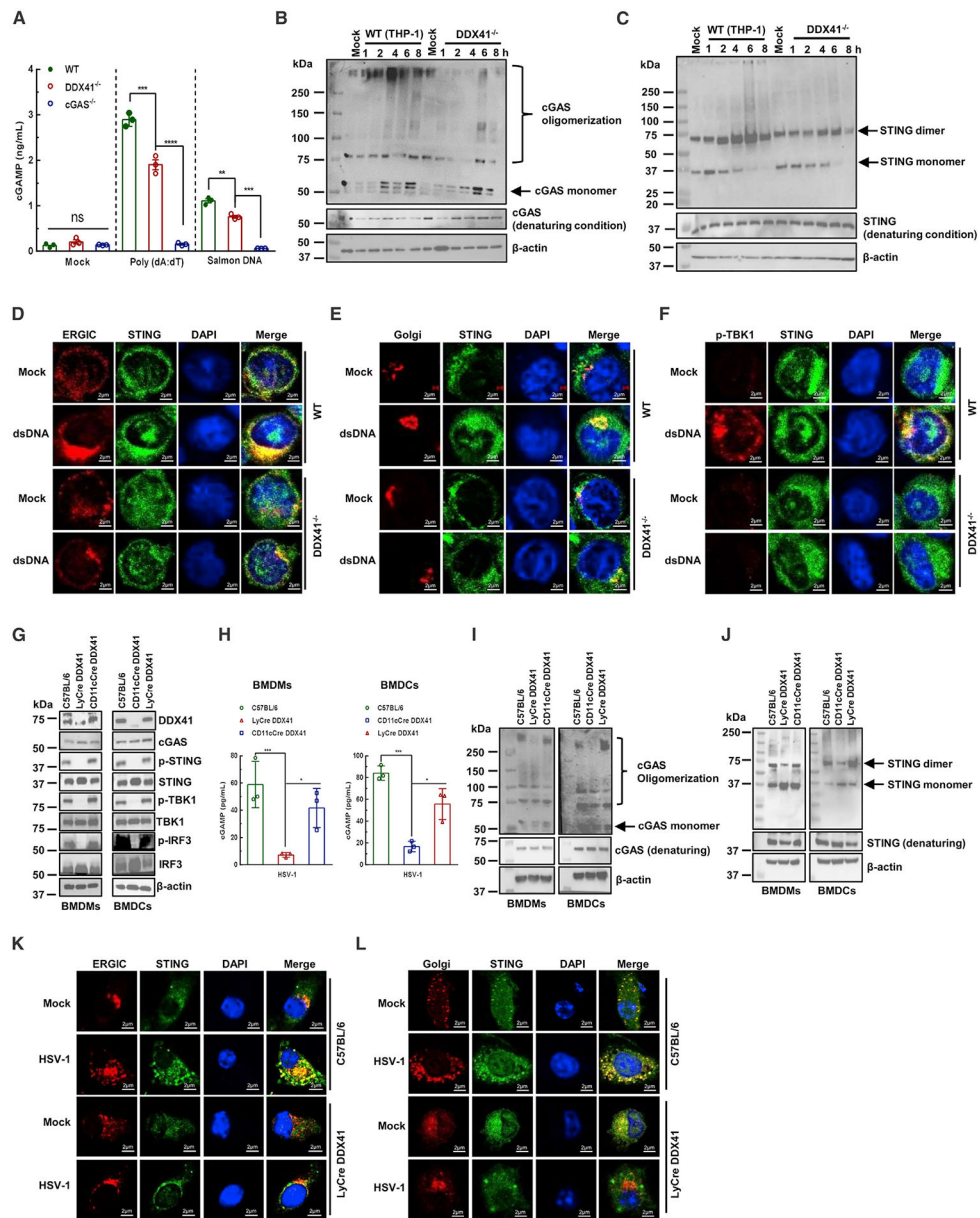


**Figure 2. DDX41 is required for the activation of cGAS and STING**

(A) cGAMP production detected by an ELISA kit (Cayman Chemical) in WT and DDX41 KO THP-1 macrophages 6 h post mock or indicated DNA stimulation. Mock (no DNA) was set as 1. cGAS KO cells serve as a negative control.

(B and C) cGAS oligomerization (B) and STING dimerization (C) status in WT and DDX41 KO THP-1 macrophages after mock or poly(dA:dT) stimulation (top). Denaturing condition and  $\beta$ -actin were used as loading controls (bottom).

(D–F) Co-localization of STING with ERGIC (D), Golgi (E), and p-TBK1 (F) in WT and DDX41 KO THP-1 macrophages after mock or poly(dA:dT) stimulation (6 h).

(G) Western blot assays of proteins in the cGAS-STING pathway after HSV-1 infection (MOI = 10, 6 hours post infection [h.p.i.] in BMDMs and BMDCs from the indicated mouse genotype.

(H–J) cGAMP production (H), cGAS oligomerization (I), and STING dimerization (J) in BMDMs and BMDCs from the indicated mouse genotype after HSV-1 infection (MOI = 10, 6 h.p.i.).

(K and L) Co-localization of STING with ERGIC (K) and Golgi (L) in BMDMs from the indicated mouse genotype after HSV-1 infection (MOI = 10, 6 h.p.i.).

For (A) and (H): data represent the mean  $\pm$  SEM of three independent experiments. \*\*\*\*p < 0.0001, \*\*\*p < 0.001, and \*\*p < 0.01.

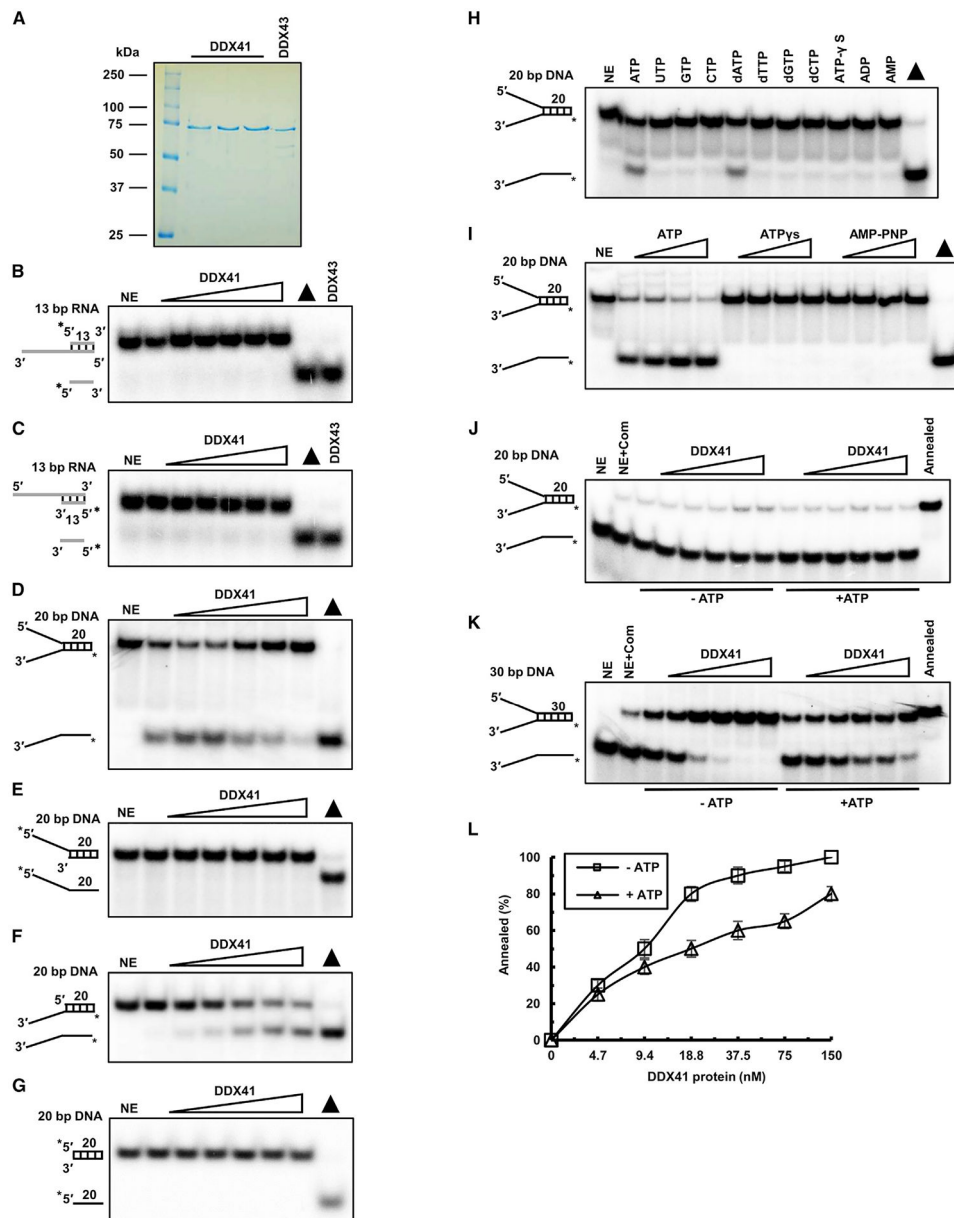


### Figure 3. Unwinding and annealing activities of DDX41 protein

(A) SDS-PAGE analysis of recombinant DDX41 proteins eluting from a Sephacryl S-300 HR column. DDX43 protein was loaded and used as a control.

(B and C) Representative images of helicase reactions performed by incubating 0.5 nM of 3'- (B) or 5'-tiled (C) 13-bp duplex RNA substrate with increasing DDX41 protein concentration (0–300 nM) at 37°C for 15 min. NE, no enzyme; filled triangle, heat-denatured RNA substrate control; DDX43 protein (300 nM) was used as a control.

(D–G) Representative images of helicase reactions performed by incubating 0.5 nM of forked (D), 5'-tiled (E), 3'-tiled (F), or blunt-ended (G) 20-bp duplex DNA substrate with increasing DDX41 protein concentration (0–300 nM) at 37°C for 15 min.

(H and I) Representative images of helicase reactions performed by incubating 0.5 nM of forked 20-bp duplex DNA substrate at 37°C for 15 min with 150 nM DDX41 protein

and different nucleoside-triphosphates (H) or with increasing concentration of ATP or ATP analogs (I).

(J and K) Representative images of strand-annealing reactions performed by incubating 0.5 nM of two ssDNAs (one of them <sup>32</sup>P labeled) for 20- (J) and 30-bp

(K) forked DNA substrate at room temperature for 30 min with increasing DDX41 protein (0–150 nM) with or without ATP (2 μM). NE + Com, no enzyme with complementary strand.

(L) Quantitative analysis of DNA annealing by DDX41 protein in (K).

Data represent the mean ± SEM of three independent experiments.

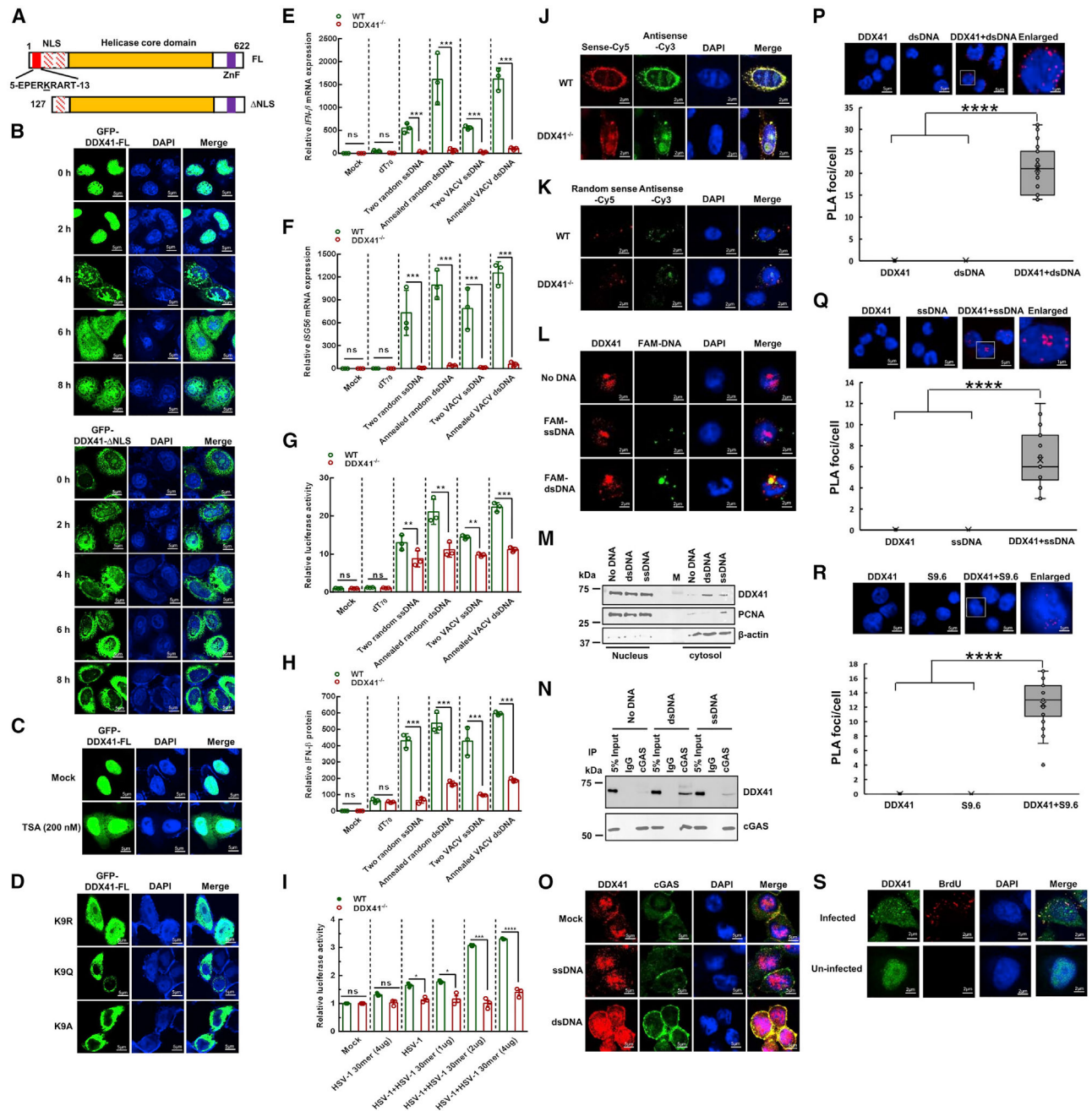
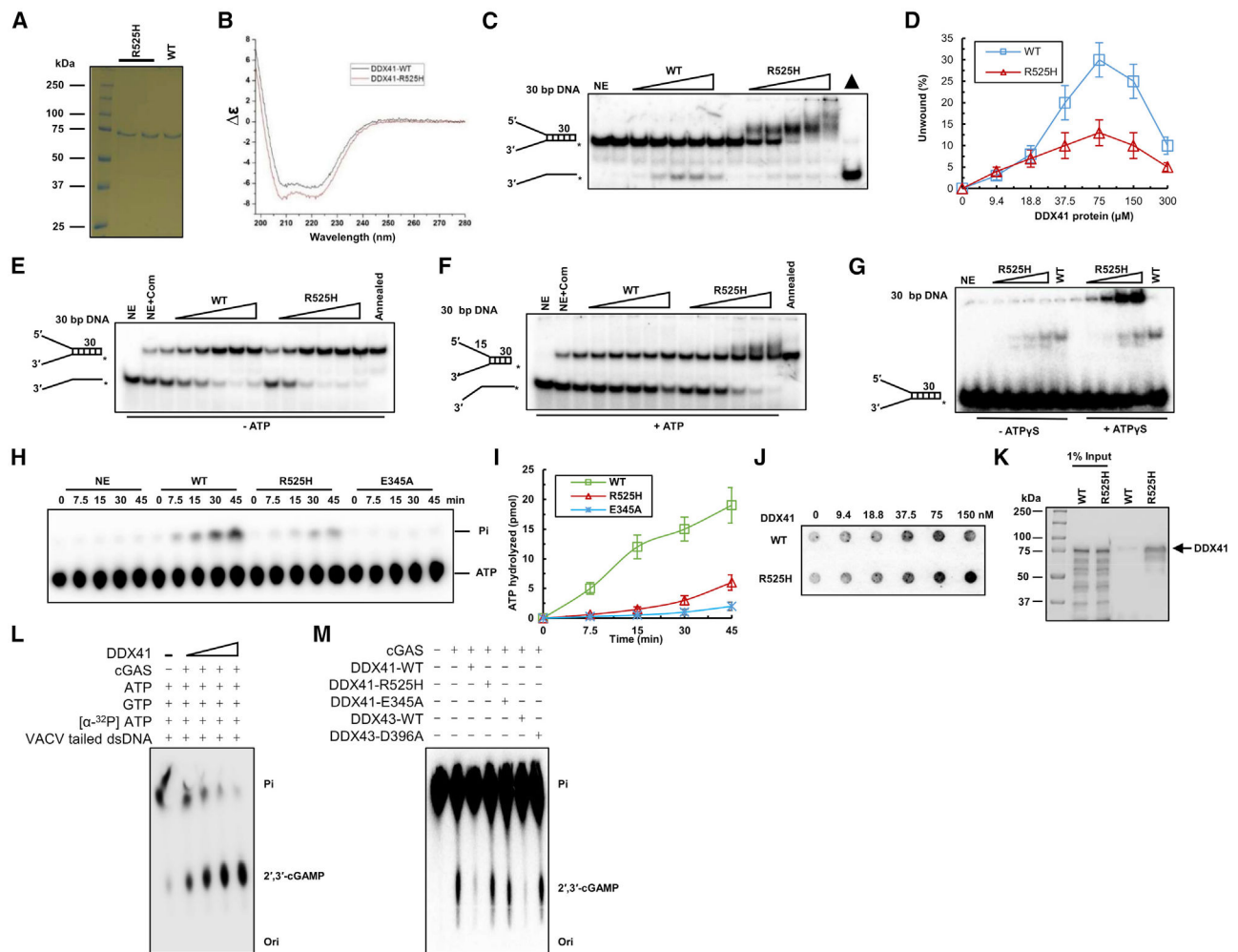


**Figure 4. DDX41 translocates from the nucleus to cytoplasm and interacts with cGAS after DNA stimuli**

(A) Schematic representation of DDX41 constructs. Three nuclear localization signals (NLSs) are indicated in red (first one solid, second and third patterned), helicase core domain in yellow, and zinc finger domain (ZnF) in purple. The sequence of the first NLS is shown, and lysine 9 is underlined.

(B) Subcellular localization of GFP-tagged DDX41 (top: full-length DDX41; bottom: NLS deletion) after poly(dA:dT) treatment in HeLa cells.

- (C) Subcellular localization of GFP-tagged DDX41 (full-length) after TSA treatment or mock in HeLa cells.
- (D) Subcellular localization of GFP-tagged DDX41 point mutants, K9A, K9Q, and K9R, in HeLa cells at 6 h post poly(dA:dT) treatment.
- (E–H) *IFN-β* (E) and *ISG56* (F) gene expression, IFN-β protein (G), and luciferase activity (H) detected in WT and DDX41 KO THP-1 macrophages after the indicated DNA treatment. Mock, no DNA; dT<sub>70</sub>; two random complementary strands: random 70-mer-T and random 70-mer-B; annealed random dsDNA: random-70mer-T and random-70mer-B annealed *in vitro*; two VACV complementary strands: VACV-70mer-T and VACV-70mer-B; annealed VACV dsDNA: VACV-70mer-T and VACV-70mer-B annealed *in vitro*. Mock was set as 1.
- (I) Luciferase activity detected in WT and DDX41 KO THP-1 macrophages 4 h after infection with HSV-1 and/or HSV-1 30-mer DNA. Mock (no DNA or virus) was set as 1.
- (J) Co-localization of two complementary DNA strands (VACV) in WT was greater than in DDX41 KO THP-1 macrophages at 4 h post transfection. Ten μg/mL DNA was used.
- (K) Co-localization of two non-complementary DNA strands in WT and DDX41 KO THP-1 macrophages at 1 h post transfection. Note: no signal was observed at 4 h post DNA transfection.
- (L) DDX41 co-localizes with FAM-labeled dsDNA (VACV) and less with ssDNA in THP-1 macrophages. Note: images of ssDNA were taken at 1 h post transfection; images of no DNA and dsDNA were taken at 4 h post transfection. FAM-ssDNA is VACV-70mer-T with F, and FAM-dsDNA is VACV-70mer-T with F and VACV-70mer-B annealed.
- (M) Western blot assays of DDX41 in the nuclear and cytosol fractions after THP-1 WT macrophages transfected with ssDNA or dsDNA. ssDNA is VACV-70mer-T, dsDNA is VACV-70mer-T and VACV-70mer-B annealed (the same for N and O).
- (N) Co-immunoprecipitation of DDX41 protein by cGAS antibody in THP-1 WT macrophages that were transfected with ssDNA or dsDNA and blotted with DDX41 (top) or cGAS antibody (bottom). Normal IgG was used as a control.
- (O) DDX41 co-localizes with cGAS after dsDNA transfection, but not ssDNA transfection, in THP-1 macrophages.
- (P–R) Representative images of PLA between DDX41 and dsDNA (P), ssDNA (Q), or DNA:RNA hybrid (R) in THP-1 macrophages, and their quantitative assays of PLA signal. 30 cells were counted in each PLA.
- (S) Co-localization of DDX41 (green) and BrdU (red, incorporated into HSV-1 genome DNA) in HeLa cells (top). Non-infection cells were used as a control (bottom).
- For (E)–(I) and (P)–(R): data represent the mean ± SEM of three independent experiments. \*\*\*\*p < 0.0001, \*\*\*p < 0.001, \*\*p < 0.01. See Table S1 for related sequence.



(G) A representative EMSA image with increasing R525H or WT DDX41 protein (0–1.5  $\mu\text{M}$ ) binding with 0.5 nM 30-bp forked DNA substrate without (left) or with (right) ATP analog ATP $\lambda$ S (2 mM).

(H) A representative image of ATP hydrolysis detected by TLC with DDX41 proteins (WT, R525H, and ATPase-dead E345A, 300 nM each) with M13 ssDNA effector (50  $\mu\text{M}$ ).

(I) Quantitative assay for the results shown in (H).

(J) A representative dot blot image of ATP bound by DDX41 proteins.

(K) ATP binding by DDX41 proteins was determined by ATP agarose (AK-102, Jena Bioscience) and followed by western blot with an anti-DDX41 antibody (SC-166225, Santa Cruz).

(L and M) TLC analysis of cGAS cyclic-dinucleotide synthesis under indicated conditions. Purified full-length human cGAS protein (2.5  $\mu\text{M}$ ), ATP (250  $\mu\text{M}$ ), GTP (250  $\mu\text{M}$ ), [ $\alpha$ - $^{32}\text{P}$ ]-ATP (10  $\mu\text{Ci}$ ), VACV tailed dsDNA (1  $\mu\text{M}$ ; Table S2), and increasing DDX41 protein (1.25, 2.5, 5, and 10  $\mu\text{M}$ ) (L). cGAS protein (2.5  $\mu\text{M}$ ) was incubated with substrate nucleotides (250  $\mu\text{M}$  each), stimulatory DNA (VACV tailed dsDNA, 1  $\mu\text{M}$ ), and DDX41 or DDX43 protein (2.5  $\mu\text{M}$ ) as indicated (M). Reactions were terminated by treatment with alkaline phosphatase to remove free nucleotide triphosphate.

For (D) and (I): data represent the mean  $\pm$  SEM of three independent experiments.

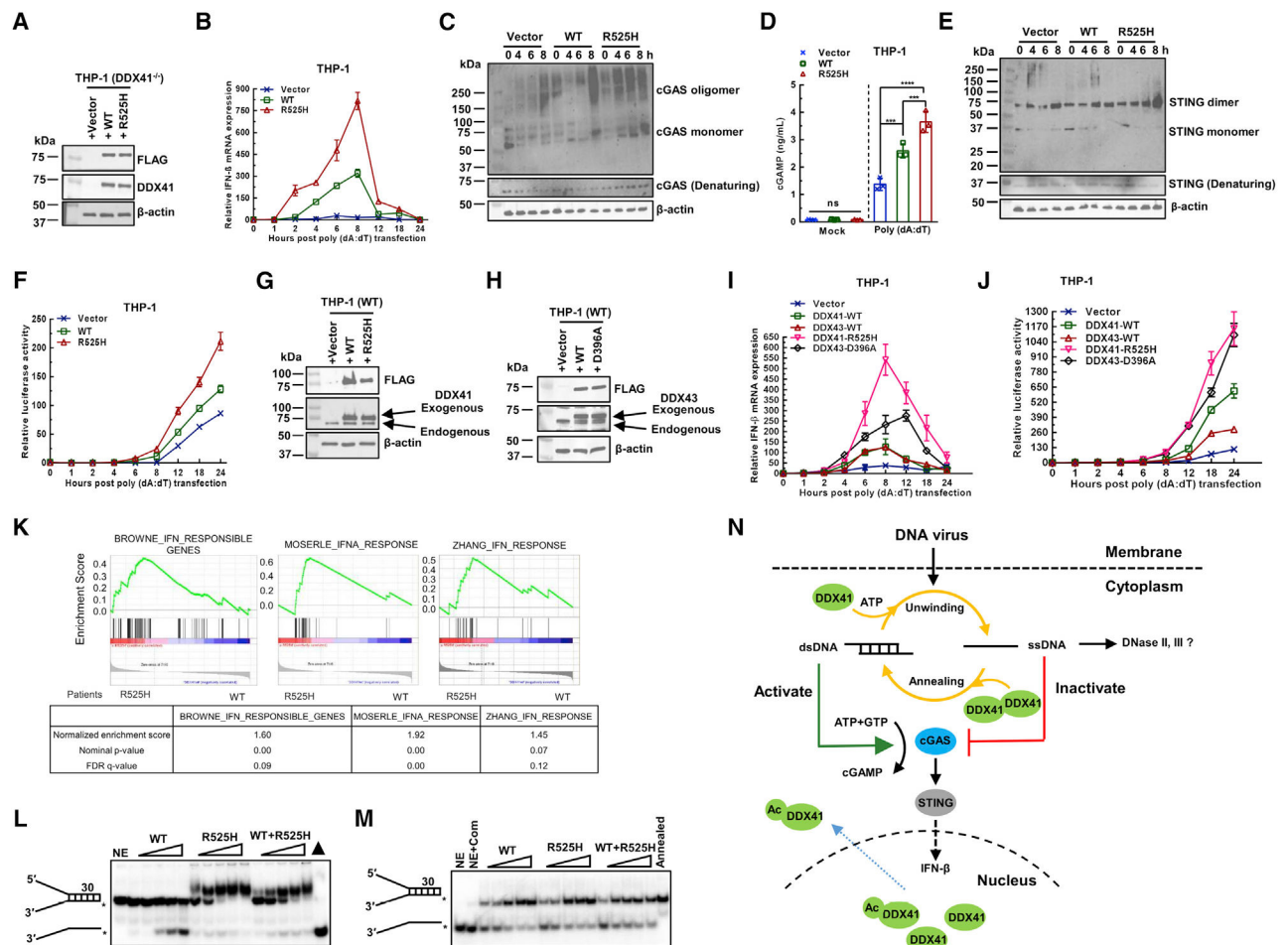


**Figure 6. Patient mutant R525H has excessive cytokine response to DNA stimulation**

(A) Western blot analysis of overexpression of vector, DDX41-WT, or DDX41-R525H in DDX41 KO THP-1 cells with the indicated antibodies.  $\beta$ -actin serves as a loading control. (B–F) qPCR analysis of the expression of *IFN- $\beta$*  gene (B), cGAS oligomerization (C), cGAMP production (D), STING dimerization (E), and luciferase activity (F) in vector, DDX41-WT, or DDX41-R525H expressed in DDX41 KO THP-1 macrophages after poly(dA:dT) treatment. For (B), GAPDH serves as an internal control, and time 0 was set as 1; for C and E, denaturing condition and  $\beta$ -actin were used as loading controls; for D, mock was set as 1; for F, time 0 was set as 1. (G and H) Western blot analysis of WT THP-1 cells expressing vector (G and H), FLAG-tagged DDX41-WT or DDX41-R525H (G), and FLAG-tagged DDX43-WT or DDX43-D396A (H), with indicated antibodies.  $\beta$ -actin serves as a loading control. (I and J) qPCR analysis of the expression of *IFN- $\beta$*  gene (I) and luciferase activity (J) in WT THP-1 macrophages expressing vector, DDX41-WT, DDX43-WT, DDX41-R525H, or DDX43-D396A after poly (dA:dT) treatment. GAPDH serves as an internal control and time 0 was set as 1. (K) Increased IFN-responsive genes occurring in R525H-expressing patient cells determined by GSEA (three patients with the R525H mutation were compared with 20

patients without the mutation). Normalized enrichment score, nominal p value, and false discovery rate (FDR) q value are indicated at the bottom.

(L) A representative image of helicase analysis on a 30-bp forked duplex DNA using indicated DDX41 proteins. Helicase reactions were performed by incubating with increasing protein (0–300 nM) and 0.5 nM duplex DNA substrate at 37°C for 15 min. NE, no enzyme. The triangle indicates heat-denatured DNA substrate control.

(M) A representative image of strand-annealing reactions using 0.5 nM two ssDNA (one labeled with <sup>32</sup>P) for forked 30-bp dsDNA substrates and DDX41 proteins (0–150 nM) without ATP. NE + Com, no enzyme with complementary strand added.

(N) A model of DDX41's role in the activation and inactivation of the cGAS-STING-type I IFN pathway. Upon DNA virus infection, DDX41 protein expression increases, and its strand-annealing activity dominates over its unwinding activity, and the produced dsDNA activates the cGAS-STING-IFN pathway. Once the virus is cleared, DDX41 expression reduces, and its unwinding activity dominates over its annealing activity, and the produced ssDNA inactivates the cGAS-STING-IFN pathway. Ac, acetylation. For simplicity, only cytosolic cGAS is shown.

For (B), (D), (F), (I), and (J): data represent the mean ± SEM of three independent experiments. ns, not significant (p > 0.05). \*\*\*\*p < 0.0001, \*\*\*p < 0.001, \*\*p < 0.01, and \*p < 0.05.

## KEY RESOURCES TABLE

REAGENT or RESOURCE	SOURCE	IDENTIFIER
Antibodies		
DDX41	Santa Cruz	SC-166225; RRID: AB_2093024
DDX41	NEB	15076S; RRID: AB_2798698
cGAS	Santa Cruz	SC-515777; RRID: AB_2734736
PCNA	Santa Cruz	SC-56; RRID: AB_628110
STING	NEB	13647S; RRID: AB_2732796
phospho-STING	NEB	19781S; RRID: AB_2737062
IRF-3	NEB	11904S; RRID: AB_2722521
phospho-IRF-3	NEB	4947S; RRID: AB_823547
TBK1/NAK	NEB	3504S; RRID: AB_225566
phospho-TBK1/NAK	NEB	5483S; RRID: AB_10693472
MAVS	NEB	3993S; RRID: AB_823565
FLAG	Sigma	F1804; RRID: AB_262044
$\beta$ -actin	Sigma	A5441; RRID: AB_476744
F4/80	Abcam	ab6640; RRID: AB_1140040
dsDNA	Abcam	ab27156; RRID: AB_470907
BrdU	Abcam	ab152095; RRID: AB_2813902
ssDNA	US Biological	D3878-16B
DNA:RNA hybrid S9.6	Kerafast	ENH001; RRID: AB_2687463
CD11c	Thermo Fisher	25-0114-82; RRID: AB_469590
Goat anti-Mouse IgG (H + L) Secondary Antibody, HRP	Thermo Fisher	31430; RRID: AB_228307
Goat anti-Rabbit IgG (H + L) Secondary Antibody, HRP	Thermo Fisher	31460; RRID: AB_228341
Alexa Fluor 488 goat anti-rabbit IgG	Thermo Fisher	A32731; RRID: AB_2633280
Alexa Fluor 594 goat anti-mouse IgG	Thermo Fisher	A-11032; RRID: AB_2534091
Bacterial and virus strains		
DH5 $\alpha$ Competent <i>E. coli</i>	NEB	C2987H
Stable Competent <i>E. coli</i>	NEB	C3040H
Rosetta 2 cells (DE3)	Sigma	71400
HSV-1 (KOS strain)	ATCC	VR-1493
Influenza A/PR/8/34 (H1N1)	ATCC	VR-1469
Chemicals, peptides, and recombinant proteins		
Lipofectamine 3000	Thermo Fisher	L3000008
Puromycin	Sigma	P9620
Polybrene	Sigma	TR-1003
Doxycycline	Thermo Fisher	BP26535
PMA (phorbol 12-myristate 13-acetate)	Sigma	P8139
Nickel Affinity beads	Sigma	P6611
dA:dT	InvivoGen	tlrl-patn-1
poly I:C	InvivoGen	tlrl-picw-250
QUANTI-Luc	InvivoGen	rep-qlc2

REAGENT or RESOURCE	SOURCE	IDENTIFIER
protein A/G agarose	Santa Cruz	SC-2003
ProLong Diamond Antifade Mountant with DAPI	Thermo Fisher	P36962
BrdU	Sigma	B5002
[ $\alpha$ - <sup>32</sup> P] ATP	Perkin Elmer	BLU003H
[ $\gamma$ - <sup>32</sup> P] ATP	Perkin Elmer	BLU502A
Clarity Western ECL Substrate	Bio-Rad	1705061
Mouse M-CSF Recombinant Protein	Thermo Fisher	RP-8615
T4 polynucleotide kinase	NEB	M0201S
Shrimp alkaline phosphatase	NEB	M0371S
DDX43 protein	PMID: 28468824; 33199368; 35257897	N/A
DDX41 protein	In this study	N/A
SUMO protease	PMID: 23209681 and in this study	N/A
cGAS protein	PMID: 31113940 and in this study	N/A
Critical commercial assays		
2'3'-cGAMP ELISA Kit	Cayman Chemical	501700
Duolink In Situ Red Starter Kit Mouse/Rabbit	Sigma	DUO92101
PowerUp SYBR Green Master Mix (qPCR)	Applied Biosciences	A25742
Deposited Data		
Raw Western blot data	Mendeley Data	<a href="https://doi.org/10.17632/4m9d4xs83j.1">https://doi.org/10.17632/4m9d4xs83j.1</a>
Experimental models: Cell lines		
HeLa	ATCC	CRM-CCL-2; RRID: CVCL_0030
HEK293T	ATCC	ACS-4500; RRID: CVCL_4V93
Vero	ATCC	CCL-81; RRID: CVCL_0059
MDCK	ATCC	CCL-34; RRID: CVCL_0422
THP-1 WT	InvivoGen	thpd-nfis
THP-1 cGAS <sup>-/-</sup>	InvivoGen	thpd-kocgas
Experimental models: Organisms/Strains		
Mouse: C57BL/6J WT	The Jackson Laboratory	JAX: 000664
CD11cCre and LyCre Ddx41 conditional KO mice	PMID: 29871919; 35303436, and in this study	N/A
Oligonucleotides		
Please see Table S1 and S2 for details, all oligos were purchased from IDT.		
Recombinant DNA		
pDEST17-DDX41	The SPARC BioCentre, the Hospital for Sick Children, Toronto, Canada	N/A
pAcGFP1-N2	Clontech	632483
pSpCas9(BB)-2A-Puro (pX459)	Addgene	62988
LentiCRISPR v2	Addgene	52961
pMD2.G	Addgene	12259
psPAX2	Addgene	12260
pRSFDuet-sumo-h-cGAS	Addgene	127161
pEN_TTmcs	Addgene	25755

REAGENT or RESOURCE	SOURCE	IDENTIFIER
pSLIK-Hygro	Addgene	25737
TOPO-TA vector	Thermo Fisher	K4575J10
pET-His-SUMO-protease	PMID: 23209681	N/A
Software and algorithms		
LSM Browser software ZEN	Zeiss	<a href="https://www.zeiss.com">https://www.zeiss.com</a>
Prism 8	GraphPad Software, Inc	<a href="https://www.graphpad.com">https://www.graphpad.com</a>
ImageQuant 5.2 software	GE Healthcare (Cytiva)	<a href="https://www.cytivalifesciences.com">https://www.cytivalifesciences.com</a>
Quantity One 1-D analysis software	Bio-Rad	<a href="https://www.bio-rad.com">https://www.bio-rad.com</a>
DICHROWEB	B.A. Wallace (PMID: 34216059)	<a href="http://dichroweb.cryst.bbk.ac.uk">http://dichroweb.cryst.bbk.ac.uk</a>
Other		
DNeasy Blood & Tissue Kit	Qiagen	69506
Superscript II Reverse Transcriptase	Thermo Fisher	18064014
QuikChange Site-Directed Mutagenesis Kit	Agilent Technologies	200523
PEI-cellulose TLC plate	J.T. Baker	JT-4473-04